BEST PRACTICE FOR MEASURING WIND SPEEDS AND TURBULENCE OFFSHORE THROUGH IN-SITU AND REMOTE SENSING TECHNOLOGIES

RJ Barthelmie

H Wang

P Doubrawa

SC Pryor*

Sibley School of Mechanical and Aerospace Engineering,
College of Engineering, Cornell University,
Upson Hall, Ithaca NY 14853
* Department of Earth and Atmospheric Sciences.
Corresponding Author: Professor R.J. Barthelmie. Email: rb737@cornell.edu

Report to the Department of Energy as partial fulfillment of grant EE0005379

http://doi.org/10.7298/X4QV3JGF

Cornell University
College of Engineering

Best Practice for Measuring Wind Speeds and Turbulence Offshore through In-situ and Remote Sensing Technologies

RJ Barthelmie

H Wang

P Doubrawa

SC Pryor*

Sibley School of Mechanical and Aerospace Engineering,
College of Engineering, Cornell University,
Upson Hall, Ithaca NY 14853
* Department of Earth and Atmospheric Sciences.
Corresponding Author: Professor R.J. Barthelmie. Email: rb737@cornell.edu

Report to the Department of Energy as partial fulfillment of grant EE0005379

July 07, 2016

Table of Contents

1 Introduction and motivation

The purpose of this document is to briefly review some applications of remote sensing technologies to atmospheric flow conditions in the offshore environment with a specific focus on the wind energy industry. Our objective is not to present a comprehensive review of the entire body of prior research on in situ and remote sensing technologies, or to describe in detail the theoretical foundations of atmospheric conditions in the marine environment. Rather, we seek to document illustrative examples of previous research, and to use those to contextualize and summarize best practice recommendations for the offshore wind energy industry.

The structure of this document is thus:

(1) We begin by briefly summarizing the motivation for making offshore wind measurements for the wind energy industry, identify the key parameters of interest, and provide a limited summary of available best practice recommendations for the offshore wind energy industry (Section 2).
(2) We then provide a précis of in situ measurement technologies, installation guidance and uncertainty analyses, and best practice recommendations (Section 3).
(3) Wind measurement devices based on optical remote sensing (ground-based, airborne, and satellite-based techniques and applications (Hasager et al. 2008)) have been extensively developed over the past thirty years, in part in response to the demands of the wind energy industry. In Sections 4 and 5, we focus on ground-based and satellite-borne instrumentation, and provide a précis of the technologies, uncertainty analyses, and best practice recommendations.
(4) We conclude in Section 6 by providing a number of recommendations for future work.

2 Context and purpose of measurements for offshore wind energy

Wind speeds offshore are typically higher and more persistent than those onshore (Pryor and Barthelmie 2001). For these and other reasons, wind turbines installations offshore are increasingly numerous (Rodrigues et al. 2015; Sun et al. 2012) and are increasing not only in number but also in size (both number of turbines deployed, and hub-height and rotor diameter) (Islam et al. 2013; Kaldellis and Kapsali 2013). There are a number of inevitable implications of these tendencies, including:

- The scale of the wind farms means that one site can not represent the conditions across the entire wind farm even in the relatively homogeneous offshore environment, particularly given that most offshore wind farms have been deployed in or close to the coastal zone (Kaldellis and Kapsali 2013) (in what has been referred to as the near-shore –i.e. within 15 km of the shore), where there is considerable spatial variability in flow regimes (Barthelmie et al. 2007; Pryor and Barthelmie 2002).
- There is a need to characterize flow not only at hub-height but across the entire swept area of the turbine rotor, so the heights at which measurements are needed is increasing.

The costs of installing meteorological masts offshore are high, and it is increasingly challenging to apply the traditional methods for accredited measurements for wind energy (i.e. mount calibrated anemometers on tall meteorological masts (Hasager et al. 2013b; Lange et al. 2004)).Hence, other tools including ground-based and satellite-borne remote sensing and modeling using either fully prognostic numerical models (e.g. numerical weather prediction models such as WRF (Hahmann et al. 2015)) or linearized/analytical models (e.g. WAsP, (Barthelmie et al. 1999)) are often used to supplement on-site measurements, for example by providing a long-term context for resource measurements or for interpolating or extrapolating between measurements at different heights or locations (Sempreviva et al. 2009).

From an engineer's perspective, a wind farm should be designed to produce as much electrical energy as possible (i.e. the wind farm layout and specific wind turbines selected for a particular deployment are selected to optimize efficient energy extraction) without compromising the structural integrity of the wind turbines (i.e. ensuring an acceptably small probability of turbine failure, wherein two failure modes can be considered; sudden exceedance of the material strength and failure due to damage accumulation). From an investor's perspective, a wind farm should be designed to maximize the profit margin. Wind is both the source of energy (revenue) and loading (expense) and error or uncertainty in measurements will increase the overall cost of energy (Lantz et al. 2012; Poulsen and Hasager 2016). Therefore, the purpose of on-site wind measurements is to provide information to help both engineers and investors to achieve their goals.

In the following sub-sections we describe the atmospheric parameters of interest to offshore wind energy in terms of quantifying power production and loads. In the subsequent sections, we describe measurement techniques available for the determination of the atmospheric variables of relevance to the wind energy industry and may also contribute to advancement of fundamental understanding of atmospheric flow in the marine environment. Although we focus exclusively here on atmospheric flow parameters, it should be noted that wave climates also comprise an important component of siting considerations for offshore wind farms, and for example, accurate estimation of wind-wave alignment, extreme wave conditions and likelihood of sea ice are also critical input parameters to site selection, project viability, and the design and operation of wind farms offshore (Larsén et al. 2015; Shaw 2012; Thomsen 2014).

2.1 Key atmospheric flow parameters for wind resource assessment and siting

According to wind energy industry guidelines (e.g. IEC (2005a)), measurements are taken to obtain the following wind parameters for offshore wind farm design:

- **Mean wind speed.** The 10-minute mean horizontal wind speed (V) is used to represent the mean motion of flow, and a detailed description of the probability distribution of 10-minute wind speeds at the hub height is the minimum requirement for wind resource assessment. The two-parameter Weibull distribution is most commonly used to represent the probability distribution of sustained wind speeds offshore (Barthelmie and Pryor 2003; Pryor et al. 2004) with typical shape factors (k) of approximately 2.0 for offshore sites (Grilli and Spaulding 2013). In locations with a large seasonal variability or a mixed wind climate, the wind speed distribution can be represented by the double-peak Weibull distribution (Burton et al. 2011).

  Although wind speeds offshore (away from the coast) do not exhibit the diurnal cycle seen onshore primarily due to the large heat capacity, seasonal variability is present as the result of the passage of synoptic atmospheric systems in combination with the seasonality in sea surface temperatures (Barthelmie et al. 1996; Emeis 2012). In the mid-latitudes there is also substantial inter-annual (and inter-decadal) variability in wind climates (Pryor and Barthelmie 2003; Schoof and Pryor 2014) due to the action of internal climate modes (e.g., North Atlantic Oscillation (Marshall et al. 2001) and El Niño Southern Oscillation (Enloe et al. 2004)) in modifying storm-tracks and frequencies. A rule-of-thumb used in the past to approximate the inter-annual variability in Europe was to assume a value of 6% variability in mean annual wind speeds (van Hulle et al. 2010). But the magnitude of the effect is likely highly geographically variable and a strong function of spatial averaging. For example, Pryor et al. (2006) used area-averaged annual wind indices to investigate inter-annual variability across Europe based on reanalysis data and found that there is a significant spatial variation and an inverse relation between latitudes north and south of 45° N. Thus wind resource estimation should optimally be based on multiple years of measurements taken at the hub height, and will be subject to increased uncertainty due to use of short measurement records. To gain information about the degree to which the in situ measurements represent the wind climate a wind farm is likely to experience (including these longer time-scales), in situ observations of offshore wind speeds can be supplemented by those derived from satellite measurements and/or modeling tools (Hahmann et al. 2015).

  Given the size of offshore wind turbines and wind farms, measurements at the hub height at a single location are not sufficient for wind resource assessment and wind farm design. The change in surface (roughness, humidity, temperature, topography) conditions from land to sea or in sea surface temperature causes the internal boundary layer to develop at offshore locations near the coast, resulting in spatial gradients of wind speed in the horizontal and discontinuity in the vertical (Barthelmie et al. 2007; Mahrt et al. 2004). Thus, far from being a uniform wind field, it is very complex to model and measure offshore wind fields, particularly in the near-shore and coastal zone. For example, sea breezes can be observed offshore at a distance of a few 100 km in tropical region and 20-50 km in mid-latitudes (Emeis 2012). Mesoscale low-level jets (LLJ) (a sharp, temporally sustained, maximum in the wind-speed profile within the lowest few kilometers of the troposphere) can extend over hundreds of kilometers in the horizontal and have been observed in a large number of coastal regions due to the thermal contrast between land and sea (Ranjha et al. 2013). At least in some locations these LLJ can be

present at heights of relevance to wind turbines (Mahrt et al. 2013; Nunalee and Basu 2014; Smedman et al. 1996). While remote sensing technologies such as lidar/sodar vertical profilers and scanning lidars are able to observe these phenomena, relatively few offshore lidar campaigns have been undertaken (Hasager et al. 2013b; Koch et al. 2012; Pichugina et al. 2012), our knowledge of their frequency, intensity and relevance for the wind energy industry remain incomplete.

- **Turbulence intensity.** Turbulence intensity (TI) is defined as the standard deviation of wind speed relative to the mean over a 10-minute period. TI is a measure of the strength of turbulent wind fluctuation and is the minimum input to simulate the turbulent wind field for wind turbine fatigue load estimation. Wind turbines are usually designed for one of the three TI categories specified using the TI at V = 15 m s^{-1} (denoted as I_{ref}) (Table 2-1). TI offshore is usually lower than those values specified in (IEC 2005a) due to the low frictional drag from the water surface (often described using the Charnock relationship (Charnock 1955)) and exhibit a complex wind speed dependence. While wind-driven waves are the main surface roughness components, offshore TI can be high at relatively low wind speeds when stability effects can be important, decreases to a minimum around wind speeds of 8-10 m s^{-1} and then increases with wind speed as higher winds speed cause a rougher sea surface (Türk and Emeis 2010; Wang et al. 2014).

Table 2-1 Parameters for wind turbine classification (IEC 2005a)

Wind turbine class	**I**	**II**	**III**
V_{ref} [m s^{-1}]	50.0	42.5	37.5
V_{ave} [m s^{-1}]	10.0	8.5	7.5
V_{g50} [m s^{-1}]	70.0	59.5	52.5
A I_{ref} [%]	16		
B I_{ref} [%]	14		
C I_{ref} [%]	12		

- **Dominant wind direction.** Understanding of the distribution of wind directions in power producing wind speeds are required as input to the optimization of wind farm design (i.e. wind turbine layout) (González et al. 2014) due to the key importance of turbine-turbine interactions (i.e. the wind turbine deep array effect) (Barthelmie and Jensen 2010). Wakes typically dissipate more slowly in the offshore environment due to the prevalence of low ambient turbulence intensity, thus DNV-OS-J101 states that "wake effects in wind farms will often dominate the fatigue loads in offshore wind turbine structures". A larger separation distance between two adjacent wind turbines can be made along the prevailing wind direction in order to reduce power lost through wake effects (Barthelmie et al. 2013).
- **Wind shear.** Wind shear (i.e. the change of horizontal mean wind speed with height) plays an important role in determining the flow across the rotor plane (and thus is an important factor in the periodic loading of a wind turbine contributing to the fatigue loads (Dimitrov et al. 2015; Sathe et al. 2013)), and is critical for vertical extrapolation of wind speeds for wind resource assessment and wind load calculation (Badger et al. 2016; Barthelmie and Pryor 2006; Hasager et al. 2013b).

  The simplest possible approach to describing the variation of mean wind speed with height is the power law:

$$V(z) = V_{hub}\left(\frac{z}{z_{hub}}\right)^{\alpha} \quad (1)$$

where V_{ref} is the wind speed at some measurement height z_{ref} and α is the power law exponent (Emeis 2012). Wind shear in the offshore wind turbine design standard IEC (2009) is specified by Eq. (1). The value of α is set to 0.14 for the "Normal Wind Profile" and 0.11 for extreme wind conditions. However, the shape of the wind profile changes with stability conditions that vary seasonally offshore and surface conditions which varies with offshore wind speed (Barthelmie et al. 2005) ; therefore, the value of α is a dynamic quantity that varies in an hourly to seasonal scale as a function of wind speed and atmospheric stability (Ernst and Seume 2012). The variation of wind speed with height can also be described using the logarithmic wind approximation, derived based on the Monin-Obukhov similarity theory (shown in (2) for neutral conditions):

$$V(z) = \frac{u_*}{\kappa}\ln\left(\frac{z}{z_0}\right) \quad (2)$$

where u_* is the surface friction velocity, z_0 is the surface roughness length, κ is the von Kármán constant (~0.4). Under non-neutral conditions, the wind profile can be modeled by adding to Eq. (2) a correction term that is a function of height and Monin-Obukhov length (Holtslag et al. 2015; Stull 1988). The logarithmic law and the associated stability correction are only valid in the surface layer which is approximately the lowest 10% of the atmospheric boundary layer (Gryning et al. 2007). Boundary-layer heights are typically lower offshore; hence, wind turbines offshore extend beyond the surface layer into the Ekman layer, and thus "unified vertical wind profile laws" that describe wind profiles above the surface layer have been developed (as described by Emeis (2014)). However, a full description of the drivers of variations in the vertical variation of wind speed in the offshore and coastal zone remains incomplete in part because of additional confounding influences from the role of humidity fluxes in dictating stability in the near-surface layer (Barthelmie et al. 2010), and the presence of internal boundary layers (due to the surface discontinuity at the coast) (Garratt 1990).

DNV-OS-J101 - Design of Offshore Wind Turbine Structures includes a guidance note that the wind speed at any height z with any averaging period T can be estimated from:

$$V(T,z) = V_{10}\cdot\left(1 + 0.137ln\frac{z}{h} - 0.047ln\frac{T}{T_{10}}\right) \quad (3)$$

Where h=10 m, T10 = 10 minutes, V_{10} = 10 m wind speed at height, h. This approximation implicitly assumes a pseudo-logarithmic profile and thus near-neutral stability and that z and h lie within the surface layer.

2.2 Extreme wind events

While the wind parameters mentioned above are necessary for energy production prediction and fatigue load estimation, the following extreme wind conditions need to be specified for wind turbine ultimate load calculation (IEC 2005a). Two types of extreme wind conditions are considered. The first type is based on the extreme value theory and it describes rare events over a period of several years (e.g., 50 year return period wind speed). The second type is related to turbulence and it represents rare events that might happen

within a 10-minute period (e.g., extreme gust). An estimate of the first type of extreme is typically derived from long-term observations of the mean wind speeds (e.g. from buoys or coastal meteorological stations), reanalysis data or targeted mesocale modeling (Larsén et al. 2013), whereas the second type is typically estimated from empirical approximations (models) and siting characteristics, since direct determination would require long-term measurements with fast response sensors such as sonic anemometers. A range of blended extremes is also considered within the wind energy industry. For example, the extreme coherent gust structure from the International Wind Turbine Design Standard IEC61400-1:2005 consists of a simultaneous gust and wind direction change as an important extreme loading case (Storey et al. 2014).

- **50-year return period wind speed.** IEC (2005a) uses the reference 10-minute sustained wind speed that has the probability of occurrence once every 50 years to specify the wind turbine class (Table 2-1); therefore, wind turbines of class I, II and III are designed to withstand the extreme wind speed 50.0, 42.5 and 37.5 m s^{-1} with the probability of once every 50 years, respectively. The classical method for this value is based on the generalized extreme value distribution fitted to annual maxima from at least 20 years of data (Coles et al. 2001), although the parameters from the Weibull distribution can be used to derive estimates of the parameters from the Gumbel distribution and thus the 50-year return period wind speed (Pryor et al. 2012). When long-term data are not available, alternative methods can be used to estimate the extreme wind speed (Coles et al. 2001; Palutikof et al. 1999).
- **Extreme gust.** Gust is the "temporary change in wind speed" and it can be "characterized by its rise time, magnitude and duration" (IEC 2005a). In the wind turbine design standard, the magnitude of the extreme operating gust is specified as:

$$V_{gust} = \mathrm{Min}\left\{1.35(V_{e1} - V_{hub}), 3.3\left[\frac{\sigma_1}{1 + 0.1d}\right]\right\} \quad (4)$$

  where σ_1 is the standard deviation of wind speed and d is the ratio of the rotor diameter to the turbulence length scale. The term V_{e1} is the 1-year return period extreme wind speed which is defined as the peak gust with *t*-second duration ($V_{g,t}$) and the running averaging time t = 3. The peak gust is commonly related to the mean and standard deviation of wind speed using the following (Holmes 2001):

$$V_{g,t} = V + g \cdot \sigma_1 \quad (5)$$

$$V_{g,t} = G \cdot V \quad (6)$$

where g is called the peak factor and G is the gust factor.

- **Extreme wind shear.** Extreme shear can lead to not only extra loading on the turbine (Sathe et al. 2013), but also reduced power production (Brower 2012). It is defined as a transient variation in the wind speed profile, either horizontally or vertically, across the rotor area (IEC 2005a). Both can be calculated from the power law exponent, hub height wind speed, turbulence parameters and the rotor diameter.
- **Extreme direction change.** The term "extreme wind direction change" here refers to an abrupt but sustained change in wind direction. Lateral and longitudinal turbulence are primary and secondary contributions to short-term direction changes (Larsen and Hansen 2008), while sustained changes in wind direction are often associated with the passage of mesoscale or synoptic meteorological fronts. A direction change faster than the wind turbine yawing speed (e.g., 0.5 deg sec^{-1} in Kim and Dalhoff

(2014)) could result in elevated loads.

2.3 Best practice recommendations

The American Wind Energy Association (AWEA) has sponsored the development of recommended practices for offshore wind turbine deployment (*Offshore Compliance Recommended Practices; Recommended Practices for Design, Deployment, and Operation of Offshore Wind Turbines in the United States* (AWEA OCRP 2012)). It mirrors the major regulatory stages framed in 30 CFR 585 (Trager 2014) and addresses most aspects of the life cycle of a wind turbine facility (excluding the initial permitting): project design and design basis; manufacturing; construction, installation, and commissioning; operation, inspection, and safety systems; and decommissioning. It is intended for use with fixed-base offshore wind structures in U.S. federal and state waters and consistent with the IEC large wind turbine standards, applies to turbines with a swept area > 200 m^2. Beyond this, and the other recommendations cited herein, there are numerous other regulations, standards, and guidelines relevant to the offshore wind industry, including:

- IEC 61400-1, Wind turbines - Part 1: Design requirements
- IEC 61400-3, Wind turbines - Part 3: Design requirements for offshore wind turbines
- IEC 61400-22, Wind turbines - Part 22: Conformity testing and certification
- ISO 19900, General requirements for offshore structures
- ISO 19902, Fixed steel offshore structures
- ISO 19903, Fixed concrete offshore structures
- ISO 19904-1, Floating offshore structures – mono-hulls, semisubmersibles and spars
- ISO 19904-2, Floating offshore structures - tension-leg platforms
- API RP 2A-WSD, Recommended practice for planning, designing and constructing fixed offshore steel platforms - working stress design.
- DNV-OS-J101 - Design of Offshore Wind Turbine Structures

3 In-situ measurements

In-situ measurements have been used in the wind energy industry for decades. Although other types of measurement support structure have been considered, in-situ measurements of wind speed and direction have typically been made by anemometers and wind vanes mounted on multiple long booms attached to meteorological masts most of which employ a lattice structure (e.g. the FINO platforms in the North Sea) (Figure 3-1). Wind speed and direction are commonly sampled every second (or more frequently in the case of the sonic anemometers) and processed to output the mean, standard deviation and maximum (minimum) for each 10-minute period (consistent with conventions summarized in section 2), which are used to estimate the probability distribution of sustained wind speeds, turbulence intensity and peak gusts, respectively. Sources of error/uncertainty in anemometry include the effects of the support structure (tower), boom and other mounting components (e.g. clamps) in addition to the anemometer design, turbulent characteristics of the flow and the instrument calibration, maintenance and challenges such as the occurrence of icing and/or deterioration of the anemometer due to erosion/corrosion (e.g. due to sea spray deposition). Therefore, best practice is required not only for good instrument design to achieve high measurement accuracy, but also for good meteorological mast design and proper instrument placement to reduce the effect of the flow interference on measurement accuracy. It is worthy of note that in addition to installations made with a primary purpose of making in situ measurements of the flow for wind energy applications, a number of resource studies have also employed wind speed and direction data from instruments mounted on buoys. For the U.S. sites these data are managed by the National Data Buoy Center, and the instrumentation and buoys are maintained by the Coastal-Marine Automated Network (C-MAN), the National Oceanic and Atmospheric Administration (NOAA) National Ocean Service (NOS), the National Weather Service (NWS), or the Great Lakes Environmental Research Laboratory (GLERL). These buoys are equipped with propeller anemometers (usually mounted at 2 or 10-m) and report 8-minute average wind speeds once hourly. The following is a brief description of in-situ measurements for offshore wind energy development for the purpose to obtain “bankable” data that must be compliant at minimum with standards issued by IEC (International Electrotechnical Commission), IEA (International Energy Agency) or MEASNET (Measuring Network of Wind Energy Institutes).

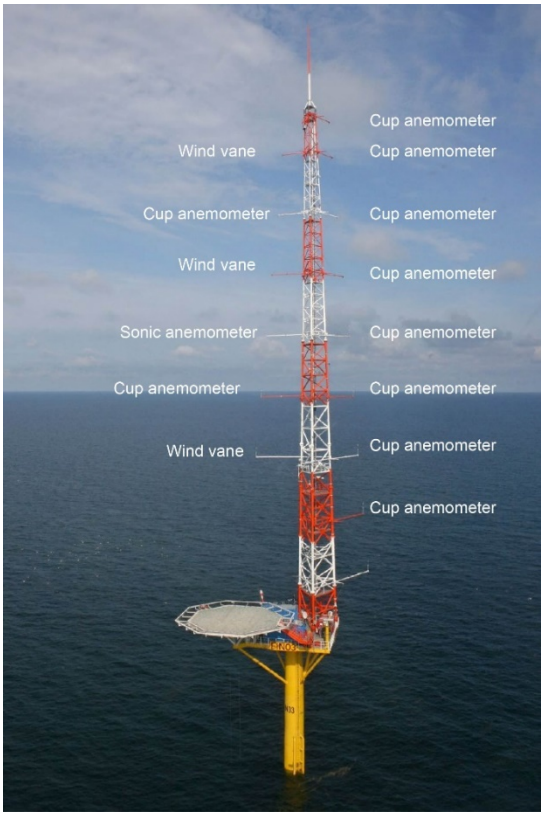

Figure 3-1 Offshore meteorological mast FINO3. (Photo source: www.fino3.de)

3.1 Instruments

A range of measurement approaches can be applied to make wind speed observations, which can be

classified according to the physical operating principle:

- pressure (e.g. Pitot tubes)
- kinetic energy (e.g. cup and propeller anemometers)
- cooling (e.g. hot wire or film anemometer)
- effective speed of sound in a moving reference frame (e.g. sonic anemometer).

Of these the majority of in situ measurements for the offshore wind energy industry conform to the second and fourth classes, although pitot tubes are have been employed for wind measurements on unmanned aerial vehicles (UAV, (Cho et al. 2011)) and on wind turbine blades and in wind tunnels during aerodynamic testing (Cooperman and Martinez 2015).

3.1.1 Cup and propeller anemometers

Properties of cup/propeller anemometers and wind vanes and guidelines on in-situ measurements are well documented (Barthelmie et al. (2005); Brock and Richardson (2001); IEC (2005b); Pedersen et al. (2006); (Wyngaard 1981), and thus they are only briefly described here. A cup or propeller anemometer is used to measure the horizontal wind speed by virtue of rotation of one component of the anemometer (Figure 3-2 and Figure 3-3), and provide a scalar mean wind speed which is lower than the vector mean (Monahan 2011). The angular velocity of the rotor connected to the cups or propeller is linearly proportional to the horizontal wind speed for the cup anemometer or the wind velocity component along the axis of rotation for the propeller anemometer. The linearity is a function of anemometer design parameters and the coefficients (i.e., the slope and intercept) should be determined individually through wind tunnel calibration. A transducer, which can be a current generator or optical/pulse counting generator, is connected to the rotor to record the angular velocity that is used to estimate the incident wind speed using the calibrated linear response coefficients.

Figure 3-2 Cup anemometer and wind vane (Source: www.campbellsci.com)

Figure 3-3 Propeller anemometer (Source: www.campbellsci.com)

Figure 3-4 The WindMaster sonic anemometer (Source: gillinstruments.com)

A typical cup anemometer has three conical or hemispherical collecting cups mounted at equal distances from a vertical shaft by equally spaced horizontal supporting arms (see comprehensive description of cup anemometer design and performance characterization given in (Kristensen 1993)). The vertical shaft rotates

on bearings arranged to cause as little mechanical loading as possible. The asymmetry of the cup arrangement ensures that the anemometer always rotates the same way irrespective of the direction of the incoming wind. While the cup anemometer is omni-directional, the propeller anemometer needs a tail vane to align the instrument with the wind direction (e.g., Figure 3-3). When the approaching flow has a non-zero vertical wind speed, the measured wind speed should ideally be proportional to the cosine of the inclination angle. However, depending on the anemometer design, the measured wind speed is usually higher than the cosine response curve, introducing an overestimation in the measured horizontal wind speed (Brock and Richardson 2001; Papadopoulos et al. 2001).

A cup or propeller anemometer does not turn at a low wind speed (e.g., < 0.5 m s^{-1}) because of internal mechanical friction. This property determines the lower threshold of the measurement range of a cup or propeller anemometer that is usually given in the anemometer specifications. There is a small range after the low threshold value over which the wind speed and angular velocity relationship is non-linear; therefore, measurements from this range are prone to errors (Brock and Richardson 2001). This non-linear range is usually not reported in the specifications. However, the lower threshold value and the non-linear range are well below 3 m s^{-1} which is commonly the minimum wind speed for energy generation; therefore, these limitations is usually not considered. The upper threshold of the measurement range is the highest wind speed that a cup or propeller anemometer can operate without damage. Note that using a measurement type with a high start-up wind speed may impact the proper fitting of the Weibull distribution (Pryor et al. 2004).

Due to the inertia of the rotating shaft, a cup or propeller anemometer also does not respond to a wind speed change immediately. This effect is quantified using a distance constant (λ_d) that is the distance the wind travels before the anemometer reaches 63.2% of a step change in wind speed, it is determined from wind tunnel tests and is highly instrument specific. This constant is shorter when wind speed increases than when wind speed decreases, causing an overestimation in the measured mean wind speed (Brock and Richardson 2001; Papadopoulos et al. 2001). For example, Filippelli et al. (2008) showed overestimation of ~1.8–3.6% in energy estimate from the NRG cup anemometer under turbulent conditions, in comparison to the Risø cup anemometer, which is known to present little sensitivity to turbulence intensity, and suggested that a linear correction may be applied to account for the overestimation. This slow (dynamic) response of a cup or propeller anemometer to a wind speed change can lead to an underestimate of the peak gust (Beljaars 1987). A cup anemometer can only measure 71% of the magnitude of fluctuating eddies with a length scale of $2\pi\lambda_d$ and less for smaller eddies (Brock and Richardson 2001). A short distance constant (i.e., a low inertia of the anemometer) is preferred and is usually achieved by reducing the distance between the cups and the rotating shaft (Emeis 2010).

According to the IEC 61400-12-1 the operational standard uncertainty of cup anemometer measurements can be derived from the classification and the wind speed bin (see discussion and application in (Friis Pedersen et al. 2006)). The operational standard uncertainty (u_i) describes the maximum deviation of the wind speed measured by the anemometer compared with the real wind speed in m s^{-1}:

$$u_i = 0.05 + 0.005 \times V_i \times {}^{k}/_{\sqrt{3}} \quad (7)$$

where V_i is the wind speed bin and k the classification. As an example the Risø P2546-OPR cup anemometer has a k value of 1.32 in flat terrain and 3.71 in complex terrain.

Calibration is required for each individual cup anemometer to define the slope and offset that linearly relate the wind speed to the angular velocity (see detailed discussion in (Eecen and Noord 2005)) and should be undertaken in a manner that complies with the standard procedure in (IEC 2005b). It is preferable for the calibration to be conducted in the wind tunnel, but calibration can also be done in the field. Calibration uncertainty comprises two components; the statistical uncertainty of the wind speed measurement and those that arise from changes in operating conditions (e.g. changes in air pressure) and factors such as digital conversion influences. Ten-minute mean wind speed measurements with well-constructed and maintained cup anemometers deployed on a support structure with minimal flow distortion in flat homogeneous terrain are highly repeatable. A comprehensive field evaluation of 37 production-mode operational cup anemometers reported correlation coefficients > 0.999895 (median value), and a standard deviation of gain values < 0.003 ms^{-1} and of offset values of ~ 0.01 ms^{-1} as measured against a reference cup anemometer. The same study found that at a wind speed of 8 ms^{-1}, the average error (again relative to the reference cup anemometer) was < 0.1% (Paulsen et al. 2007). Due to wear and tear, an aging cup anemometer is likely to experience deviation from the originally calibrated transfer function (Pindado et al. 2012). Therefore, frequent recalibration and maintenance maybe necessary to ensure high accuracy of cup anemometer measurements at a frequency dependent on their type and deployment context. Deployment and maintenance of meteorological instrumentation in marine environments is particularly challenging due to deposition of sea spray on instruments and the associated corrosion. Thus more frequent replacement/maintenance of cup anemometers (and other equipment) may be required to ensure high accuracy measurements.

3.1.2 Wind vanes

A wind vane is commonly a flat plat that can rotate to align with the wind direction (Figure 3-2). The flat plat is usually balanced by a counterweight on the other end (Figure 3-2). Wind vanes operate on the principle that the dynamic pressure due to the wind causes a static force on a plate if the plate is not exactly aligned with the wind direction. The direction of the arm of a mechanical wind vane is typically determined from a mechanical switch, or an optical encoder, or a precision potentiometer. A good wind vane should be statically balanced and have a low inertia of momentum, a low bearing friction, and a high damping ratio such that the wind vane will not overshoot too much when wind direction changes. The most common source of error is misalignment (to the North) during installation.

3.1.3 Sonic anemometers

A sonic anemometer measures the travel time of an acoustic signal over a fixed path between a pair of transducers oriented into different directions (e.g., Figure 3-4) to determine the wind velocity component parallel to the path that can in combination be used to measure the three components of wind velocity in addition to the virtual temperature at high frequency (10–50 Hz, Kochendorfer et al. (2012)) and therefore can respond to rapid flow variations. Sonic anemometers can be deployed to measure mean horizontal wind speeds with very high accuracy and at high frequency (Coquilla et al. 2010) (permitting detailed description of gusts). The ability of 3-D sonic anemometers to accurately measure changes in wind direction and gusts, and their resistance to mechanical failures and icing, spurred the US National Weather Service to change all Automated Surface Observation Systems (ASOS) to ice-free sonic anemometers during the early 2000's. They also permit quantification of higher moments of the 3-D flow and the vertical heat and momentum fluxes. Sonic anemometers have no movable parts; hence, they are more durable and require less maintenance than cup and propeller anemometers. However, sonic anemometers are not accurate in rain

and are subject to flow distortion due to the probe head that influence the accuracy of the fluxes, vertical velocities and high-order moments of the horizontal flow. The transducers upwind of a sonic anemometer can cause flow distortion, affecting the measurements from the downwind transducers. The flow distortion depends on the arrangement of the transducers (i.e., orthogonal and non-orthogonal arrangement) and the turbulence intensity (Kochendorfer et al. 2012). While the flow distortion can be minimized by proper placement of the transducers, wind tunnel calibrations can provide correction algorithms to account for the effect of flow distortion on measurements (Grelle and Lindroth 1994; Nakai and Shimoyama 2012). If a sonic anemometer is tilted, there can also be cross-contamination in the velocity components and variations in horizontal flow can be erroneously recorded as fluctuations in the vertical velocity (Wilczak et al. 2001). The factory calibration for this effect is normally performed in low turbulence conditions in a wind tunnel and does not hold in more turbulent conditions (Högström and Smedman 2004). Therefore, it is important to apply corrections to the measurements if turbulent conditions are experienced. Vickers and Mahrt (2006) found that vertical wind speeds are sensitive to the tilt correction applied to the measurements from sonic anemometers. Moreover, because the corrections are based on the assumption of zero long-term vertical wind speed, they do not allow for vertical motion from "persistent horizontal divergence". They found that the "tilt angle method" (Kyaw Tha Paw et al. 2000) produced the smallest errors, but suggested using data from several anemometers and mass continuity to estimate the vertical wind speed whenever possible as this was the method that produced the most realistic results.

3.2 Installation and operation

Because cup anemometers are the most commonly used instruments for offshore wind energy development, here we focus on deployment for this type of anemometer and direct the reader to Aubinet et al. (2012) for discussion of sonic anemometer installation and operation.

Flow interference with the meteorological mast is a major error source for in-situ measurements (Fabre et al. 2014; Westerhellweg et al. 2012). Given the measurement heights required for offshore wind energy applications, lattice masts (Figure 3-1) are most commonly used to support meteorological instrumentation at different heights, although a range of mast structures is available (including solid cylindrical towers). As mentioned above, the meteorological mast causes flow distortion, resulting in upwind retardation, lateral acceleration and downstream wake when the air passes the mast (Hansen and Pedersen 1999) (Figure 3-5) (see detailed discussion in IEC 61400-12 Annex G – Mounting of instruments on the meteorological mast). The effect of the downwind wake from the support structure will always exist, although the amount of distortion depends principally on the solidity of the mast and installed objects, and can be minimized by careful mounting of cup anemometers. A simple solution to minimize wake effects is to install two cup anemometers on alternate sides of the meteorological mast and conditionally sample the resulting data streams to obtain a free-stream wind speed according to the wind direction. If one of the anemometers fails, correction can still be made with models developed from the observations made when both anemometers were working (Farrugia and Sant 2013; Westerhellweg et al. 2012). Note that IEC (2005b) requires two cup anemometers with the same design at each height for consistency verification. In general, placing anemometers sufficiently far away from meteorological masts and booms can reduce the effect of the lateral acceleration and upwind retardation.

Consistent with the discussion above, wind speed measurements from cup anemometers have the following five types of uncertainties (IEC 2005b):

- The uncertainty related to the calibration before a measurement campaign. This type of uncertainty is evaluated using the standard errors of the calibrated slope and offset from several wind tunnel tests.
- The uncertainty related to the calibration after a measurement campaign. The post calibration checks whether there is any variation in the slope and offset used during the measurement campaign. The maximum difference (up to 0.2 m s^{-1}) between the wind speed based on the pre- and post- calibration should be used to quantify this type of uncertainty.
- The uncertainty related to a cup anemometer's operational characteristics such as the distance constant. This type of uncertainty is quantified in terms of cup anemometer classification. A cup anemometer is classified in terms of the class type and class number. The class type specifies the site conditions (e.g., flat or complex) in which a cup anemometer is used. Different site conditions imply different mean wind field and turbulence conditions. The class number represent the maximum deviation of cup anemometer measurements from the calibrate values. This number is usually derived from numerical simulation with specific external conditions by manufacturers and needed for uncertainty calculation. For more details, reader can refer to Annex I in IEC (2005b) and Pedersen et al. (2006).
- The uncertainty related to the mounting of a cup anemometer. Without mast flow distortion correction 1.5% uncertainty needs to be added to cup anemometer measurements. If flow distortion correction is applied, the uncertainty level can be reduced. Methods for estimating flow distortion can be found, for example, in Westerhellweg et al. (2012) and Farrugia and Sant (2013).
- The uncertainty related to the acquisition of data from cup anemometers.

In addition to those instrument-related uncertainties, atmospheric turbulence can also introduce uncertainty in the derived statistics such as the mean and standard deviation of wind speed. This type of uncertainty is a function of the turbulence integral time/length scale given the averaging period is fixed to 10 minutes (Lenschow et al. 1994). The implications of these error sources (most of which also apply to other types of anemometers) are firstly that they should be considered when selecting an instrumentation suite and support structure and undertaking operational maintenance of offshore deployments, and secondly that they should be fully considered when using such observations for wind energy applications.

3.3 Best practice recommendations

Anemometer calibration and other requirements have been articulated in a number of international standards (and in recommendations from the National Institutes for Standards and Technology (e.g. NIST Handbook 150)). For example:

- IEC 61400-12-1, "Power Performance Measurements of Electricity Producing Wind Turbines", articulates procedures for performance evaluation of a wind turbine, and also discusses the requirements for performing anemometer calibrations along with tests to evaluate instrumental sensitivity to terrain and atmospheric conditions.
- ASTM D5096-02, "Determining the Performance of a Cup Anemometer or Propeller Anemometer", describes the procedure for determination of the Starting Threshold, Distance Constant, Transfer Function, and Off-Axis Response of a cup anemometer or propeller anemometer from direct measurement in a wind tunnel.
- ISO 17713-1, "Meteorology – Wind Measurements Part 1: Wind Tunnel Test Methods for Rotating Anemometer Performance". This standard was last reviewed in 2016 and describes wind tunnel test methods for determining performance characteristics of rotating anemometers, specifically cup

anemometers and propeller anemometers. It also describes an acceptance test and unambiguous methods for measuring the starting threshold, distance constant, transfer function and off-axis response of a rotating anemometer in a wind tunnel.

- ASTM D6011-96, "Determining the Performance of a Sonic Anemometer/Thermometer". This test method covers the determination of the dynamic performance of a sonic anemometer/thermometer that employs the inverse time measurement technique for velocity or speed of sound, or both. Performance criteria include: (a) acceptance angle, (b) acoustic pathlength, (c) system delay, (d) system delay mismatch, (e) thermal stability range, (f) shadow correction, (g) velocity calibration range, and (h) velocity resolution.
- ISO 16622, "Meteorology – Sonic Anemometers/Thermometers – Acceptance Test Methods for Mean Wind Measurements", defines test methods of the performance of sonic anemometers/thermometers. It is applicable to designs measuring two or three components of the wind vector within an unlimited (360°) azimuthal acceptance angle.

There are also a number of best practice recommendations regarding instrument deployment on meteorological masts. The International Electrotechnical Commission specification IEC 61400-12-1 proposes a mathematical model for anemometer boom lengths to minimize upstream and downstream flow distortions based on computational fluid dynamic simulations. IEC (2005b) recommends that flow distortions due to the meteorological mast should be kept below 1.0% which requires a boom-mounted anemometer to be no closer than 6 times the mast width (i.e., $6R_b/L_m$ in Figure 3-5). IEC (2005b) provides formulas to calculate the separation distance between the meteorological mast and the measurement point for both tubular towers and lattice masts required for a given accuracy. The IEC standard also requires cup anemometers to be mounted at least 20 times the boom diameter above the boom to achieve <0.5% distortion.

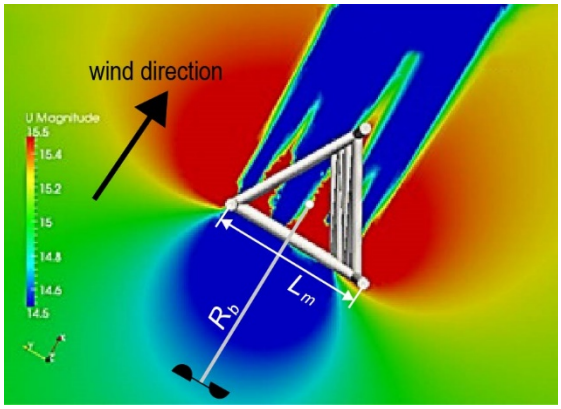

Figure 3-5 Simulated wind speed around the lattice meteorological mast used at FINO3 from Fabre etal. (2014). The freestream wind speed is 15 ms^{-1}.

4 Ground-based remote sensing

Ground-based remote sensing technologies (e.g. Radar (RAdio Detection And Ranging), Sodar (SOnic Detection And Ranging) and Lidar (LIght Detection And Ranging)) measure the motion of air using the Doppler effect induced by wind tracers on electromagnetic waves. These instruments compare the Doppler-shifted frequency between the original and the reflected signal. This frequency shift is transformed to a line-of-sight velocity, the magnitude of the wind velocity along the beam direction. Thus, if the light or sound is sent at different angles relative to the zenith, the line-of-sight velocity can be decomposed into the three wind speed components using the geometry of the scanning configuration.

Both radar and sodar emit wavelengths similar to the size of turbulent eddies and measure the reflection off the varying temperature structure in the atmosphere, while lidars use laser light in the infrared range and use reflection from atmospheric particles. Doppler radar technologies have not been extensively employed in the wind energy industry (Hirth et al. 2015), and the authors are not aware of any deployments in the offshore environment beyond the Radar@Sea experiment reported in (Trombe et al. 2014). Sodars have been more extensively employed for atmospheric flow quantification (Bradley (2007); Doviak and Zrnić (1993); Emeis (2011); (Rodrigo et al. 2013)), and for wake studies in offshore wind farms (Barthelmie et al. 2003; Barthelmie et al. 2006), and are available from a number of commercial vendors (e.g. Remtech, Atmospheric System Corporation, Metek, Scientec, Second Wind). A number of previous analyses have focused on discussion of the relative merits of sodars and lidars and inter-comparison of the resulting wind speed estimates (Bradley et al. 2012; Hasager et al. 2008; Lang and McKeogh 2011). Because of the great potential of, and increased industry interest in, Doppler lidars and an increasing number of deployments in offshore and coastal locations (Hasager et al. 2013b; Hasager et al. 2008), herein we focus on Doppler lidars.

4.1 Lidars

Herein we focus on Doppler lidars, but note the existence of direct detection lidars that are also based on transmitting laser pulses into the atmosphere, but instead of recording the Doppler shift, only the backscatter intensity is used to reconstruct the wind speed and direction (e.g. Pentalum Technologies Spidar lidar) (Afek et al. 2013). The sampled time series represents the aerosol backscatter (and thus aerosol density) along the line of sight of the transmitted pulse. The wind speed and direction are derived by tracking aerosol structures, and correlating the backscatter intensity in different locations and times.

Static and scanning ground-based (as well as nacelle-mounted) Doppler lidars have been extensively employed in fundamental studies of the wind turbine inflow (Wagner et al. 2009) and investigations of the downstream wake field characteristics (Barthelmie et al. 2014). Nacelle mounted lidars have also been exploited for wind forecasting, power curve assessment (Wagner et al. 2014) and adaption of feed-forward control strategies (Mikkelsen 2014; Simley et al. 2014).

The major components of a Doppler lidar are shown in Figure 4-1. The lidar generates and emits a laser beam into the atmosphere. Aerosols in the laser beam path backscatter the light and their motions cause a Doppler frequency shift (Δf) in the backscattered beam. Using these aerosols as wind tracers, the lidar detects the Doppler frequency shift in the returned signal to estimate the radial velocity (v_r) which is the component of wind velocity in the direction of the line of sight (LOS) (Figure 4-1):

$$v_r = \boldsymbol{n} \cdot \boldsymbol{v} \tag{8}$$

where $\boldsymbol{v} = (u, v, w)$ is the 3-component wind vector and $n = (\cos\phi \sin\theta\,, \cos\phi \cos\theta\,, \sin\phi)$ is the unit directional vector representing the orientation of the laser beam. Here ϕ is the elevation angle and θ is the azimuth angle of the laser beam. Because the emitted laser pulse has a finite spatial extent, the backscattered radiation received at any moment is from a collection of aerosols illuminated by the laser pulse. Therefore, a radial velocity (v_R) measured at a location is a volumetric average of radial velocities within a probe volume centered at that location.

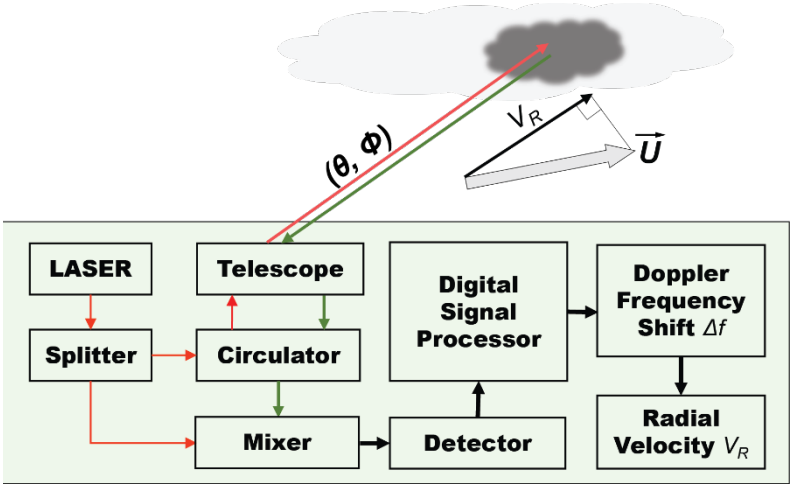

Figure 4-1 Schematic drawing of Doppler lidar and its wind measurement principle (see also Figure 4-2).

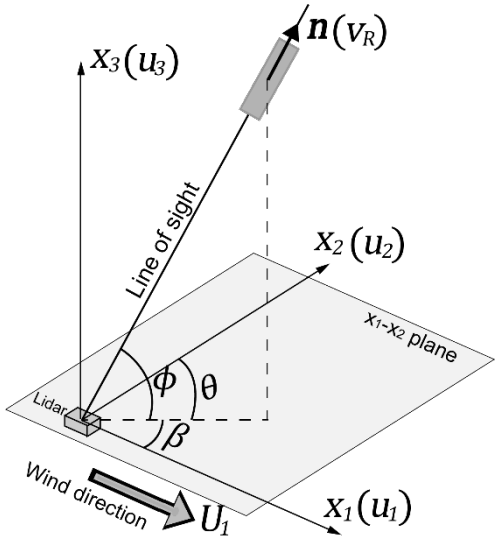

Figure 4-2 Schematic of the coordinate system employed in Eq. (8) where u_1=u, u_2=v and u_3=w.

4.1.1 Lidar types

Doppler lidars can be sub-classified in terms of the duration of laser emission:

- A *pulsed* lidar emits a laser pulse of high energy characterized by its wavelength (λ_L), pulse duration (τ_L) and pulse energy (E_L). The returned signal is sampled with a sampling interval T_s and the range distance of the n^{th} sample is resolved as $cnT_s/2$ where c is the speed of light. Samples are binned/gated

with the bin size *M*. A spectrum is estimated for each gate and a radial velocity is derived from the spectrum to present the wind velocity at the center of that range gate. A *pulsed* lidar can provide radial velocity measurements at multiple range gates simultaneously, but the quality of measurement deteriorates with increasing range distance because the signal weakens according to the inverse square law.

- A *Continuous Wave (CW)* lidar measures radial velocity by detecting the Doppler frequency shift in the backscattered signal from continuously emitted laser beams with stable power. It processes the returned signal from a volume centered at the laser focal point; therefore, a *CW* lidar measures the radial velocity at only the focal point at one time.

In terms of functionality, there are currently vertical profiling lidars and scanning lidars:

- *Vertical profiling lidars* are specifically designed to measure vertical profiles of wind velocity up to heights of about 200 m with vertical resolution of about 20 m. They are easy to set up and provide ready-to-use wind velocity measurements. The most widely used vertical profiler lidars in wind energy are the ZephIR300 and WINDCUBE v2.
- *Scanning lidars* can probe the atmospheric flow in any direction usually in the hemisphere above the lidars using a two-axis optical scanner. Scanning lidars can measure wind velocities on a horizontal plane, on a vertical plane or in 3-dimenional space. However, in order to make a good use of scanning lidars, expertise is needed in terms of scanning geometry design and post data processing. Commercially available scanning lidars include Galion, Halo, WINDCUBE and WindTracer.

4.1.2 Lidar design

Lidars are designed to satisfy the following requirements from end users: (i) spatial resolution, (ii) sampling rate, (iii) measurement accuracy and (iv) maximum range. Therefore, lidar design parameters are described below in terms of these four design aspects:

Spatial resolution: There are two types of spatial resolution. The first is geometric resolution (Δp) which is the separation between two measurements. A *CW* lidar realizes its geometric resolution by rapidly adjusting its focal length, while the geometric resolution of a *pulsed* lidar is the size of a range gate determined by the sampling rate (T_s) and the sample number (M) per gate. The second spatial resolution is the physical resolution (Δr) that represents the spatial extent of a radial velocity measurement. For a *CW* lidar the physical resolution increases quadratically with the focal length (Ahn and Fessler 2003; Sonnensc and Horrigan 1971). For example, for the ZephIR, Δr increases from 7.5 m to 58.4 m when the focal length increases from 50 m to 150 m. The physical resolution for a pulsed lidar is the sum of the geometric resolution and the width of the emitted pulse (Banakh and Smalikho 2013) and therefore it is invariant with range distance. The resolutions above are defined for the measured radial velocity on laser beam direction and they are often called the probe volume of lidar measurements. In practice, wind velocities are estimated from a scanning geometry that covers a large volume in the atmosphere, which is referred to as the measurement volume.

Temporal resolution: A radial velocity is commonly derived from an averaged spectrum to improve the measurement accuracy. The averaging period defines the temporal resolution of a lidar measurement, although it should be noted that this will differ greatly from the temporal resolution when the measurement volume is considered. For a *CW* lidar, each individual spectrum is derived from the signal in a time window;

hence, its temporal resolution is the total time spanned by time windows used for averaging. A *CW* lidar represent instantaneous wind velocities and can have a very high temporal resolution (e.g., 0.002 seconds or 500Hz sampling frequency for the *CW* WindScanner from DTU-Wind (Risø)). For a *pulsed* lidar, each individual spectrum is derived from the signal from one laser pulse returned from a range gate; therefore, its temporal resolution is determined by the number of pulses used for averaging (typically of the order of 1 second) and the pulse repetition frequency which specifies the number of laser pulses emitted per second by the lidar.

Data quality: For a *pulsed* lidar, assuming no turbulence in the probe volume, the quality of a measured radial velocity in terms of its standard error can be approximated with the following equation (Frehlich and Yadlowsky 1994; Pearson and Collier 1999):

$$\sigma_{r,SNR} = \frac{\lambda_L/10}{\sqrt{N_{eq}}}\left(\frac{1}{\Phi \cdot \Omega} + 1.42\right) \tag{9}$$

- $N_{eq} = N_L \cdot M_s t_s \cdot \tau_L$ is the equivalent sample number over which the averaging is taken. Here N_L is the number of spectra or laser pulses giving the averaged spectrum, $M_s t_s$ is the observation time of a measurement from a range gate, and σ_L is a measure of the correlation time scale of the pulse profile.
- $\Phi = M \cdot \mathrm{SNR}$ represents the "effective number of photoelectrons coherently detected per observation time" (Frehlich and Yadlowsky 1994). SNR is the signal to noise ratio.
- $\Omega = 0.11 M_s t_s/\sigma_L$ represents the independent sample numbers of the signal per range gate.

The equation above illustrates that spectrum averaging (increasing N_L) can reduce the standard error. All parameters except SNR in Eq. (9) are determined through lidar design. SNR is the ratio of the average heterodyne signal power to the average noise power and it can be estimated using the following equation (Huffaker and Hardesty 1996):

$$SNR = \frac{\eta_L \beta_a T_a^2 c P_L \sigma_L}{h\nu B_w} \frac{\pi d^2}{r^2}\left[1 + \left(\frac{\pi d^2}{\lambda r}\right)^2 \left(1 - \frac{r}{d_f}\right)^2 + \frac{2d^2}{\rho_0^2}\right]^{-1} \tag{10}$$

where η_L is overall system efficiency, β_a is the atmospheric backscatter coefficient, T_a is the one-way atmospheric transmission, $h\nu$ is the photon energy, B_w is the receiver bandwidth. The term ρ_0 is the turbulence parameter which for a constant refractive index structure function (C_n^2) is given by:

$$\rho_0 = \left(\frac{21.47 C_n^2 r}{\lambda_L^2}\right)^{-3/5} \tag{11}$$

Comparison between the observed SNR (median of 4600 observations) and the predicted SNR from Eq. (10) are shown in Figure 4-3. The agreement is very good even with the assumption that the backscatter and absorption coefficients are constant. The deviation of the peak location from the focal distance is due to the large C_n^2 at this measurement site.

Turbulence in the probe volume can add uncertainty to the measured radial velocity, giving the following approximation for the standard error in turbulent wind field (Huffaker and Hardesty 1996):

$$\sigma_r = \sqrt{\sigma_{r,SNR}^2 + \sigma_{r,v}^2/N_L} \tag{12}$$

where $\sigma_{r,v}^2$ is the variance of radial velocity in the probe volume. Based on the above it is clear that for a given lidar, accuracy of lidar radial velocity measurement mainly depends on the aerosol concentration in the atmosphere in terms of the backscatter coefficient and the atmospheric transmission coefficient. The focal length can be adjusted in order to improve the accuracy at a location or region of interest.

For a *CW* lidar, because the signal is mainly from the focal point, its measurements always have high SNR and therefore sufficient accuracy if other assumptions are valid in the probe volume (e.g., uniform wind field in the probe volume).

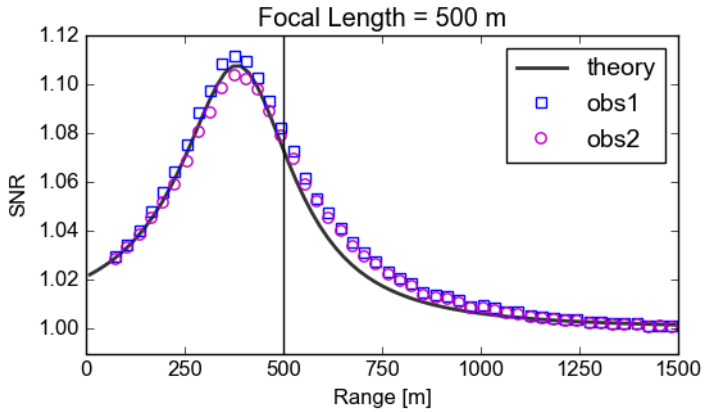

Figure 4-3 SNR and range relationship derived from the medians of 4600 measurements from two days and predicted using Eq. (9).

Maximum range: The maximum range is defined here as the range distance beyond which the measurement uncertainty (the standard error) is higher than a threshold value. Because of the relationship between the standard error and SNR, SNR is typically used to set up a threshold value to filter bad quality data. A threshold value of SNR is usually recommended by lidar manufacturers (e.g., -20dB for the Galion lidar). The dependence of SNR on the aerosol properties seen in Eq. (9) illustrates that the maximum range varies with atmospheric conditions such as aerosol backscatter, turbulence refractive index and humidity (Aitken et al. 2012).

4.2 Installation and operation

To retrieve wind velocities from the lidar-measured radial velocities, a lidar measurement involves (i) designing a scanning geometry to measure radial velocities and (ii) applying an inverse method to estimate wind velocities. Details of scanning geometry design and wind velocity retrieval for single lidar applications are given in this section. Here we are assuming that the lidar is ground-based. For discussion of nacelle-based lidar operation see

4.2.1 Calibration and accuracy

Each lidar should be calibrated to verify the sampling rate T_s and the orientation of the laser beam. For *CW* lidars, accuracy of the focal range needs to be checked because it defines the range of any measurements. For *pulsed* lidars, the trigger time needs to be calibrated to a high accuracy because it is used for range gate determination in combination with the sampling rate. Lidar calibration is typically done by detecting the

speed and location of a well-controlled moving belt in a laboratory setting, use of wind tunnels is typically not possible due to the probe volume size, and thus the accuracy of retrieved wind speeds has most frequently been undertaken using field experiments relative to other lidars or cup or sonic anemometers.

In the field, IEC standard IEC 61400-12-1 2005 provides a procedure to define the accuracy class for ground-based lidar used for 10-minute mean wind speed measurements over flat terrain (see summary in Figure 4-4). In brief in the relative lidar error is derived from the difference between wind speed measurements from lidars and cup anemometers with high accuracy and is assumed to have linear relationships with the environmental variables such as wind shear and turbulence intensity. This assumption is the result of numerous lidar verification studies (e.g., Gottschall et al. (2012); Lindelöw et al. (2008)). Then ordinary least squares regression is applied to each pair of an environmental variable and the relative error to estimate the slope. Based on the significance of the fit, only the influential environmental variables are kept. The sensitivity of lidar measurements to an environmental variable is then defined as the product of the fitted slope and a given range of that environmental variable. The final accuracy class is defined as the half of the quadrature sum of the sensitivities of all the influential variables. The standard requires the accuracy class of a specific lidar should be given by applying the same procedure (given in **Error! Reference source not found.**) by at least three lidars at two sites.

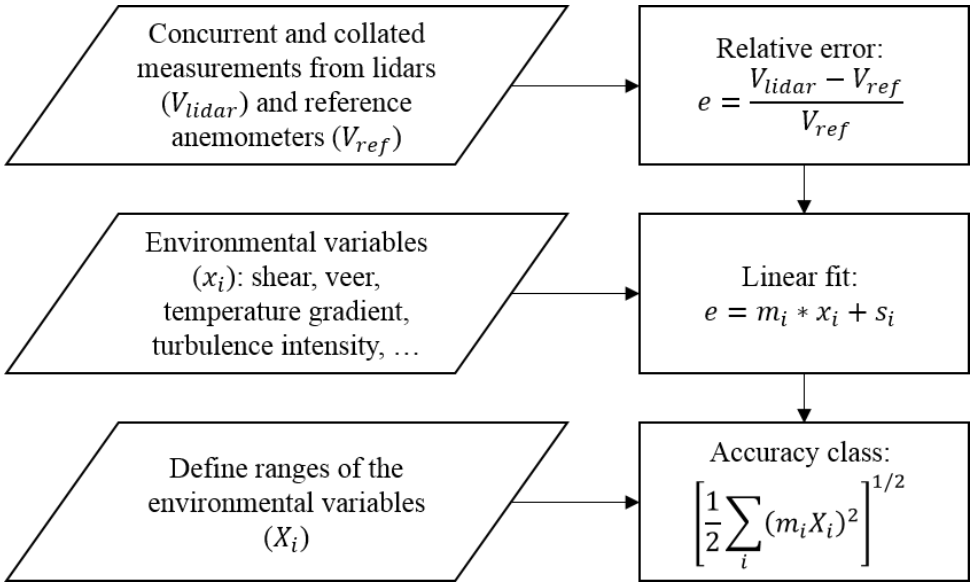

Figure 4-4 Flowchart of the procedure for lidar accuracy classification

4.2.2 Installation and scanning geometry design

To meet a measurement purpose, a scanning geometry is configured on a lidar during site installation. Range height indicator (RHI) and plan position indictor (PPI) are the two basic scanning geometries that can be used to form other complicated scanning geometries. A PPI scan varies the azimuth angle with a fixed elevation angle and therefore takes measurements on a conical surface (Figure 4-5). Single stack PPI scans are commonly used to study flow structures on horizontal planes such as wind turbine wakes (Aitken et al. 2014; Wang and Barthelmie 2015) and 2-dimensional mountain flows (Choukulkar et al. 2012). A low elevation angle should be used for these applications such that the scanned conical surface is

approximately flat. Radial velocities at the same range can be used to estimate the horizontal wind speed at the height associated with that range; this is the so-called arc scan method (Wang et al. 2015). A low elevation angle is preferred for arc scan applications in order to reduce the effect of non-zero vertical velocity on the estimated wind speed. An RHI scan obtains observations on a vertical slice in the atmosphere by varying the elevation angle with a fixed azimuth angle (Figure 4-6) and are used for investigating flow structures on vertical planes. RHI scans have been used to study the structures and dynamics of low level jets (Banta et al. 2002) and evolutions of vortices in the wake of an aircraft (Köpp et al. 2004) and in the lee of a mountain (Weissmann et al. 2009).

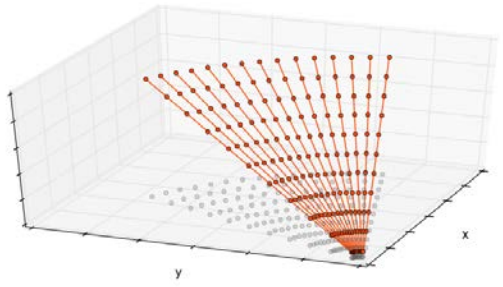

Figure 4-5 Plan position indicator (PPI) scanning geometry schematic

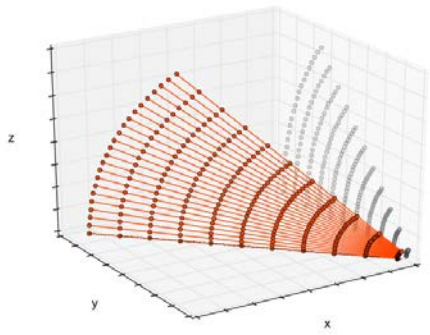

Figure 4-6 Range height indicator (RHI) scanning geometry schematic

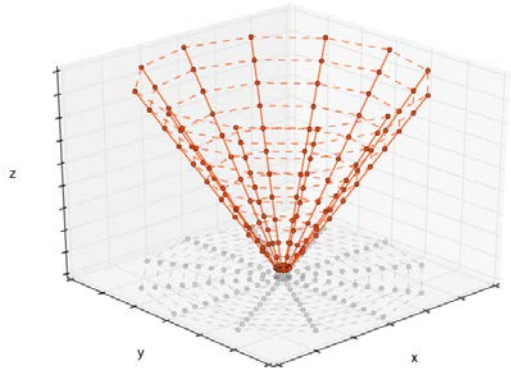

Figure 4-7 Velocity-azimuth-display (VAD) scanning geometry schematic

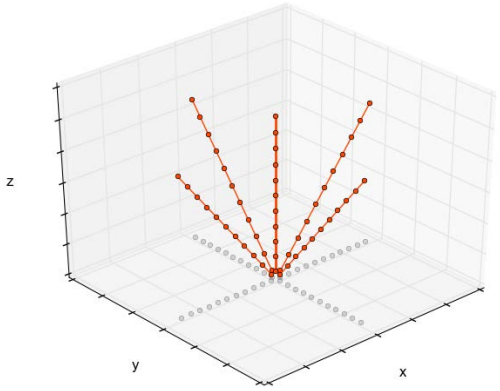

Figure 4-8 Doppler-beam-swing (DBS) scanning geometry schematic

Vertical profiles of wind speed can be obtained with the velocity-azimuth-display (VAD) technique (used by ZephIR) or the Doppler-beam-swing (DBS) techniques (used by WINDCUBE). The VAD technique that uses PPI scans with 360° azimuth span (Figure 4-7) was first developed to estimate vertical profiles of wind speed from radar (Browning and Wexler 1968) and has been widely used in wind energy to measure vertical wind shear (Emeis et al. 2008; Peña et al. 2015b). The DBS technique swings the laser beam at the four cardinal directions and the vertical direction sequentially (Figure 4-8). Vertical wind speed is directly measured with the vertically-pointing beam and then the west-east and south-north wind components are deduced from radial velocities.

Compound scan geometries can be formed with a combination of the four scanning geometries above to

achieve different measurement purposes (Clifton 2015). For example, Banta et al. (2002) used the VAD technique to estimate wind directions to control the azimuth angle of RHI scans for measuring the vertical structure of wind speed. Krishnamurthy et al. (2013) used multiple stack PPI scans to derive the wind speed distribution on a terrain-following surface for wind resource assessment. Compound scans allow observations of complex flows, but they require more sophisticated algorithms to retrieve wind velocities.

The azimuth and elevation angles associated with measurements are recorded with respect to the local east-north-up coordinates. Therefore, during installation, it is necessary to align the lidar with the true north and level the lidar with the local earth surface. Otherwise, the registered measurements are taken at locations different those expected which introduces errors. Lidars are usually equipped with levels or accelerometers for leveling (pitch and roll). A common method of wind direction alignment for scanning lidars is to use a nearby wind turbine or meteorological mast as a reference hard-target.

Doppler lidars deployed offshore (typically on support platforms provided by purpose built meteorological masts or transformer or oil/gas platforms), where the assumption of horizontal homogeneity generally realized, yield accurate estimates of wind speeds. Typical doppler lidars have a footprint of approximately 1×1 m^2 and a weight of 50 kg. The major challenges to these deployments are generally presented by the power requirements (most Doppler lidars require 50 to 100 W of power, more if heating or cooling is required) and the need to elevate the lidars above the heights that could be impacted by waves and in a fashion where the support structure does not interfere with the line of sight (Courtney and Hasager 2016). Doppler lidars have generally been deployed on fixed platforms, though there have been some ship deployments (Pichugina et al. 2012) and there have been a small number of deployments of vertical pointing lidars on buoys (Mathisen 2013). All commercially available floating lidars are based the technologies from ZephIR and WINDCUBE but with different designs of the floating platforms and algorithms to compensate for the motion of the ocean (Courtney and Hasager 2016).

4.2.3 Wind retrieval

Quality control should be applied to exclude lidar measurements with large potential errors. Most procedures exclude data with low SNR (since low SNR indicates poor signal quality and large measurement uncertainty) and strong returns from hard targets.

Wind velocity retrieval is an inverse process that is straightforward in simple flows but is still an ongoing research topic in complex flows. Simple flows usually allow simple assumptions of the flow structures that enable the use of linear least squares methods. The most common assumption is for a horizontally homogeneous wind field that is valid for flows over flat and homogeneous terrain. If this assumption is valid, the VAD technique is very accurate in retrieving wind velocities (Browning and Wexler 1968). Vertical profilers use the VAD technique; hence, their measurements are accurate and reliable over flat and uniform terrain (Peña et al. 2015b). A vertical pointing beam can be added to VAD scans to provide direct measurement of vertical wind speed to reduce the uncertainty in estimating the vertical wind speed from VAD scans. Because the mean vertical wind speed is close to zero in the atmosphere, it can typically be neglected in wind velocity retrieval (Wang et al. 2015). The assumption of a uniform wind direction can sometimes be made for simple flows. With an additional assumption of zero vertical wind speed, wind velocity retrieval is reduced to the following equation:

$$V_H = -\frac{v_R}{\cos\phi\cos(\theta - \theta_w)} \tag{13}$$

where θ_w is the wind direction. This method was used to observe low level jets from RHI scans in Banta et al. (2002) and wind turbine wake characteristics in Wang and Barthelmie (2015). Boccippio (1995) assumed that the wind field over a small region is linear and retrieved the flow divergence and deformation from lidar measurements. The same linear wind field assumption was used in Krishnamurthy et al. (2013) to estimate wind velocities on terrain-following surfaces.

For complex flows, lidars can provide qualitative observations of flow patterns using RHI and PPI scans, but it is still challenging to derive accurate wind velocities quantitatively due to the inhomogeneous and non-stationary nature of complex flows (Clifton 2015). In order to measure vertical profile of wind speed over complex terrain with vertical profilers, Bingöl et al. (2009) developed a method which estimates the errors of the VAD technique at a site with complex terrain using flow modeling and derives correction factors to correct measurements from vertical profilers at the site. Weissmann et al. (2009) used the continuity equation to identify vortices from radial velocities from RHI scans with the assumption that the RHI scan is aligned with the mean wind direction (i.e., 2-dimenional flow). Aitken et al. (2014) assumed that the wind turbine wake has a Gaussian deficit profile and estimated the main wake characteristics such as the wake center and wake width from PPI scans by fitting the measured radial velocities to a Gaussian function. Advance methods were studied by Chai et al. (2004) who assimilated the measured radial velocities with the 4-D data assimilation method to estimate a time evolving 3-dimensional flow field. Based on the existing applications of single lidars in complex flows, wind retrieval methods in complex flows rely on the assumptions of flow structures that can be simple analytical models or complicated computational fluid dynamics (CFD) models. Applying these flow models also introduces uncertainties and difficulties. Dual-Doppler and triple-Doppler, described below, are alternative solutions for lidar measurements in complex flows that are less dependent on assumptions regarding flow structures.

It is possible to derive turbulence statistics of atmospheric flows from lidar measurements, but lidar turbulence measurements are less established than mean wind field measurements (Mann et al. 2010; Newman et al. 2016; Sathe et al. 2015). Methods for applying lidar to derive higher moments of the flow and challenges to improved measurement accuracy can be found in (Sathe and Mann 2013; Wang et al. 2016b). Turbulence measurements from the vertical profilers are subject to two error source: volumetric averaging of radial velocity measurements that reduces variance, and scanning geometry that causes cross contamination in velocity variance estimates (Sathe et al. 2011). The cross contamination can be avoided by estimating turbulence statistics directly from radial velocity variance using, for example, the six-beam method for the Reynolds stress (Sathe et al. 2015), fixed azimuth RHI scans for the streamwise velocity variance (Banta et al. 2006), and four-orthogonal RHI scans for the momentum flux and heat flux (Gal-Chen et al. 1992). However, these methods do not account for the volumetric averaging effect and hence will underestimate turbulence statistics. Thus, a turbulence model needs to be applied to compensate for the volumetric averaging effect. For example, an isotropic turbulence model was used to estimate the turbulence kinetic energy dissipation rate from lidar measurements (Banakh et al. 1999; Frehlich and Cornman 2002), while Sathe et al. (2011) used the Mann turbulence model (Mann 1994) to investigate the question “can lidar measure turbulence?”. Branlard et al. (2013) developed and proved a method to approximate the wind speed distribution with the mean lidar spectrum for CW lidar. With this method,

radial velocity variance can be directly derived from the wind speed distribution without attenuation by the volumetric averaging.

4.2.4 Uncertainty quantification

Lidar wind measurement is an inverse process; therefore, its uncertainty originates from the measured radial velocities and propagates to the estimated wind velocity through the inverse process. Each measured radial velocity can be decomposed into four components as expressed by the following equation:

$$v_R = v_{R0} + v_R' + e_m + \delta_m \tag{14}$$

where:

- v_{R0} is the expected radial velocity and its definition depends on the purpose of measurements. In the case of vertical profilers for wind resource assessment, v_{R0} is the 10-minute mean radial velocity associated with a beam orientation.
- v_R' is the fluctuation component due to turbulence. If the purpose of measurements is the instantaneous wind velocity at a location, this term is equal to zero. However, if the purpose is to measure the mean wind velocity, this term is the major source of uncertainty (Wang et al. 2016a).
- e_m is the random error in radial velocity measurements. This random error is the result of the radial velocity estimation from the discretely sampled returned signal and its standard deviation is mainly a function of SNR and independent sample number used for radial velocity estimate (Frehlich and Yadlowsky 1994).
- δ_m is the bias in radial velocity measurements. Radial velocity estimate assumes that in the probe volume the wind field is homogenous and stationary and aerosols are evenly distributed. Wind shear violates this assumption and introduce bias in radial velocity measurements. Weak signal can also cause bias (Frehlich and Yadlowsky 1994).

The errors mentioned above will propagate to the estimated wind velocity through the inverse method. If the errors in the measured radial velocities are known, the uncertainty in the estimated wind velocity can be derived using existing error propagation theory. However, often time additional errors will be introduced and should be accounted for when the assumptions made for the inverse method is not valid. Therefore, uncertainty quantification of lidar measurement requires knowledge of external conditions such as wind shear, veer and turbulence. For applications of vertical wind profilers over flat terrain, readers should refer to IEC 61400-12-1 2015 for uncertainty quantification methods. For lidar applications in complex flows, it is difficult to evaluate the uncertainty of lidar measurements with reference anemometers because the spatial coverage of lidar measurements is much larger than anemometers. Researchers have used the measurements from one lidar to evaluate the wind velocities retrieved from other lidars positioned at a different location (Xia et al. 2008). Another method is to take virtual lidar measurements in a wind field simulated with large eddy simulation models and evaluate the uncertainty or performance of a scanning geometry and a wind velocity retrieval method by comparing the retrieved wind velocities with the “true” wind velocities from the simulation (Stawiarski et al. 2015).

Multiple studies have evaluated lidar (and sodar) retrieved horizontal wind speeds relative to cup and sonic anemometers (Table 4-1) and have sought to make recommendations to optimize scan geometries to improve the accuracy of the wind speeds (e.g. (Wang et al. 2015)).

Table 4-1 Summary of some previous in-situ evaluations of lidar with a focus on offshore deployments and studies that have presented the evaluation using linear regression fits relative to well-maintained anemometers.

Reference	Site description and reference anemometer	Lidar description	Performance evaluation metrics
(Wang et al. 2015)	National Wind Technology Center (NWTC) in Colorado. Complex terrain. Sonic and cup anemometers	Sgurr scanning Doppler lidar, operated with arc scans	Regression fit to 10-minute mean wind speeds $y=1.063x-0.202$ ($R^2=0.956$) RMSE = 0.72 ms^{-1} Bias = 0.09 ms^{-1}
(Peña et al. 2009)	Transformer platform at the Horns Rev offshore wind farm. Cup anemometers	ZephIR vertically pointing lidar	Regression fits to 10-minute mean wind speeds from 3 different anemometers $y=0.96x+0.16$ ($R^2 = 0.97$) $y=0.99x+0.09$ ($R^2 = 0.98$) $y=0.99x+0.11$ ($R^2 = 0.97$)
(Peña et al. 2015a)	FINO-3 offshore platform, multiple cup anemometers	WindCube pulsed vertically pointing lidar	Regression fits to 10-minute mean wind speeds from 2 different anemometers $y=1.04x+0.09$ ($R^2 = 0.98$) $y=1.03x+0$ ($R^2 = 0.98$)
(Emeis et al. 2007)	Høvsøre coastal mast, cup anemometer at 100-m	ZephIR vertically pointing lidar	Regression fit to 10-minute mean wind speeds $y = 1.0038x+0.0793$ ($R^2 = 0.9882$)

4.3 Dual lidar and triple lidar techniques

One of the challenges for single lidar applications is the retrieval of the 3-component wind velocities from the measured radial velocity. There is always uncertainty in making assumptions required for wind velocity retrievals in complex flows (as described above), but lidars are poised to become the best instrument for observing the spatial variability of complex flows regardless. The solution to this challenge is the dual-lidar and triple-lidar techniques which directly measure two and three components of the wind velocity at one location simultaneously from non-collocated two and three lidars, respectively. The dual or triple lidar techniques do not require the flow homogeneity assumption employed for single lidars.

Three types of dual lidar techniques have been applied and tested in various field experiments. The first one is the virtual tower technique first used by Calhoun et al. (2006) and Collier et al. (2005) to measure wind speed profiles in the urban atmospheric boundary layer. Virtual towers are formed on the intersecting lines of RHI scans made by two non-collocated lidars. By assuming zero vertical wind speed, the horizontal wind velocity can be directly measured at locations where the beams from the two lidar intersect. The virtual tower technique, as shown in Figure 4-9, can be used to measure wind velocity profiles offshore by placing two lidars on the coast. The second dual lidar technique is the coplanar technique (Hill et al. 2010). Two non-collocated lidars are coordinated to perform RHI scans with the same azimuth angle. The RHI scans are aligned with the baseline connecting the two lidars so that radial velocities are measured on a coplanar vertical plane. The horizontal and vertical components on the plane can be retrieved without any assumptions. Therefore, the coplanar technique is suitable for studying flow structures in vertical planes such as the mountain waves (Hill et al. 2010) and downslope flows (Cherukuru et al. 2015). The third dual lidar technique is able to observe wind velocities in a 3-dimensional space using two non-collocated lidars

performing scans that overlap (Drechsel et al. 2009; Newsom et al. 2015). A Cartesian grid is created to fill the overlapped area. Radial velocities from the two lidars are interpolated to the grid points using the weighted sum of radial velocities within a predefined volume. The two-component horizontal wind velocities can be directly derived on each grid point from the radial velocities of the lidars by assuming zero vertical wind speed. Three-component wind velocities can also be retrieved with the physical strain of the continuity equation, for example, using the Multiple Doppler Synthesis and Continuity Adjustment Technique (MUSCAT) (Bousquet and Chong 1998). Uncertainties of dual lidar techniques can be found in Stawiarski et al. (2013) and they are mainly related to the scanning geometry configurations. One common issue of dual lidar techniques, which was experience in several dual lidar applications, is the difficultly of synchronizing two lidars. Because of the probe volume and the different scanning geometries configured on different lidars, beams from two lidars can intersect within a spatial and temporal window. Therefore, wind velocities from dual lidar measurements are temporal averages, which require the assumption of stationarity.

The triple lidar technique can directly measure the instantaneous wind velocity by pointing their beams at the same location and was tested recently as a solution for wind measurements over complex terrain (Wang et al. 2016c). A synchronized triple lidar system with a centralized computer controlling the orientations of the beams from the three lidars has been recently developed Vasiljevic (2014) and applied to quantification of the spatial variability of near-surface flow (Berg et al. 2015).

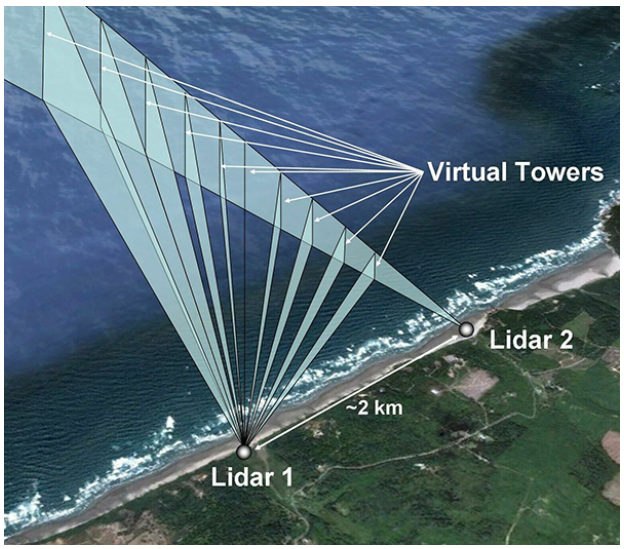

Figure 4-9 Schematic of the dual lidar virtual tower technique for offshore wind measurements (Image source: www.pnnl.gov)

4.4 Best practice recommendations

At the same time as the use of lidar in wind energy changes and becomes more sophisticated, standards and best practice are being developed as listed below although these are not specifically for offshore. Some individual agencies and companies have also produced ‘best practice type guidelines’ (Clive 2011a, 2011b; Ecofys 2013; GLGH 2012):

- While most wind energy standards are produced by IEC under the 61400 series, currently the only standard for use of remote sensing devices is for power curve measurements and this is described in IEC 61400-12-1 Draft Annex L.
- DNV have produced recommended practice guidelines for remote sensing for wind energy assessment (DNV 2011)
- MEASNET have included brief practical guidelines for lidar and sodar (MEASNET 2009)
- IEA Task 32 is dedicated to the exchange of ideas, experiences and techniques of measurements with lidar http://www.ieawindtask32.org/ and is summarized in http://www.ifb.uni-stuttgart.de/IEAWindTask32/Docs/Task32_FinalReport_finaldraft.pdf (Kuhn et al. 2015) and is divided into 3 parts:
  I. Calibration and classification of lidar devices
  II. Procedures for site assessment
  III. Procedures for turbine assessment

  These are also subdivided so that in addition to general practice for ground based lidar and nacelle-mounted lidar, working groups have addressed issues of particular relevance to offshore including use of floating lidar, http://www.ieawindtask32.org/wp-content/uploads/2016/04/IEA-StateOfArtFloatingLIDAR-2Feb2016_v1.0.pdf

  The most comprehensive recommended practice report is by IEA Task 32 Working group. Although it is not specifically for offshore there are 44 recommended practices for the use of vertically-pointing ground-based lidar. The report and can be downloaded from: http://www.ieawind.org/index_page_postings/RP/RP%2015_RemoteSensing_1stEd_8March2013.pdf (Clifton et al. 2013).

5 Satellite-based remote sensing

Ocean wind mapping has been undertaken using passive microwave SSM/I (Special Sensor Microwave/Imager), scatterometer and synthetic aperture radar (SAR) (Hasager et al. 2013a). The principle of operation of passive microwave SSM/I retrieval of wind speed is based on the concept that the amount of microwave energy emitted from the ocean surface is a function of wave structure and foam coverage which are, in turn, dictated by the near-surface wind speed (Goodberlet et al. 1989; Mears et al. 2001). The biggest advantage of SSM/I is the long available data record (1987 onwards) but only wind speed is retrieved and the coverage is poor in the coastal zone, thus this product has not been widely used in the wind energy industry. Both wind scatterometers and SAR are active microwave radars that emit microwave pulses and measure the intensity of their reflection from the ocean/water surface. The intensity of the backscattered signal, which is quantified by the normalized radar cross section (NRCS), is related to sea surface roughness elements consisting of capillary and short-gravity waves that are generated by surface wind stress. Wind retrieval is based on Geophysical Model Functions (GMFs) that are empirically developed relationships between the wind velocity and NRCS (Hersbach et al. 2007; Stoffelen and Anderson 1997). The physical basis for GMFs is the relationship between the surface friction velocity and NRCS. The retrieved wind speed at 10 m above the sea surface is estimated assuming the logarithmic wind profile (section 2). Because microwave radiation can penetrate clouds and precipitation, satellite-borne radar sensors can provide observations under all weather conditions. The technical comparison between the wind data from scatterometer and SAR is given in Table 5-1 (Badger et al. 2012). Advantages and disadvantages of wind data retrieved from these two radars and their applications in wind energy (which are largely confined to wind resource assessment and full array wake studies) are described in following two sub-sections (see a comprehensive list of dataset available for resource assessment given in (Shaw 2012)).

Table 5-1 Technical specification of wind data from scatterometer and synthetic aperture radar based on (Badger et al. 2012).

	Scatterometer	Synthetic Aperture Radar
Output parameters	Wind speed and direction	Wind speed
Wind retrieval	Data providers	Users
Spatial resolution	25 km	0.5 km
Spatial coverage	Daily global	Selected area
Coastal mask	<70 km from coastline	None
Temporal resolution	2 per day	Variable, < 1 per day
Temporal coverage	Continuously since 1991	ERS 1/2 since 1991/1995
Current sensors	ASCAT, OSCAT, HY2A, MetOp-B	Envisat ASAR Radarsat-1/2
Rain sensitivity	High-rain flags provided	Low

5.1 SAR

A full description of SAR-based wind observations is provided in Dagestad et al. (2013), here we focus on providing a brief précis of satellite-borne SAR for wind energy applications.

The main advantage of SAR is its high spatial resolution (<500 m) that enables observations of mesoscale flow structures and wind speed near the coast offshore. Raw data from providers such as the European Space Agency (ESA) are calibrated and geocoded by users first and then wind speed is retrieved mainly

using the following tools: the commercial software SARTool and the APL/NOAA SAR Wind Retrieval System (ANSWRS) developed by the Applied Physics Laboratory at John Hopkins University. Currently, a priori knowledge of wind direction is needed for SAR wind retrieval because NSRC is acquired from a single antenna. The input wind direction is most commonly derived from either:

- The orientation of km-scale streaks visible on SAR images. The orientation of these streaks is aligned with wind direction, and they can be identified with imaging processing methods such FFT (Furevik et al. 2002), wavelet methods (Fichaux and Ranchin 2002) and gradient methods (Koch 2004). However, because wind direction 180° can cause the same streak orientation, there is 180° ambiguity.
- Numerical weather prediction models. For example, the APL/NOAA Wind Retrieval System (ANWRS) uses wind direction from the Global Forecast System (GFS) to retrieve wind speed from *Radarstat-1/2* data (Monaldo et al. 2014).
- Scatterometers, if a SAR and scatterometer overpass each other simultaneously (He et al. 2005).
- In-situ measurements where they are collocated with the SAR image (Christiansen et al. 2006).

New retrieval methods without required wind direction input can be found in (Dagestad et al. 2013).

The swath width is relatively narrow for SARs (100−500 km) (Dagestad et al. 2013). The narrow swath causes the sample number of SAR-based wind speed observation to be low at one location since the overpass rate is low. The sample number can be further reduced during winter time if the area included in SAR images has ice coverage. For example, it takes one day to acquire one sample at high latitude under the large swath mode and more than five days at the equator for the RADARSAT-1 (RSI 1995). There were only 1009 samples and 63−102 samples per month in total from 2003 to 2010 useful for wind resource assessment in the Baltic Sea (Hasager et al. 2011). Nonetheless, new instruments are being launched increasing the number of scenes available.

Wind speed retrieval from SAR images is limited to the range 2−24 m s^{-1}. The estimated wind speed from SAR data has a standard deviation of about 1.0−2.0 m s^{-1} when evaluated against in-situ measurements and model predictions (Hasager et al. 2008). Comparison with cup anemometer wind speeds versus SAR at Egmond aan Zee and Horns Rev found linear regression fits (and R2) and root mean squared error (RMSE) of; y=0.91x+0.42 (R^2=0.81) RMSE = 1.47 ms^{-1}, and y=0.98x-0.14 (R^2=0.88) and RMSE = 1.26 ms^{-1} (Hasager et al. 2015). The main source of uncertainty is the wind direction used for wind speed retrieval. For example, wind direction gradient in a SAR pixel can cause errors since uniform direction is assumed for wind retrieval. Errors are also introduced when atmospheric stability is not neutral because wind speed at 10 m height is based on extrapolation using the logarithmic law. If present, obstacles cause high returns and hence introduce positive bias.

SAR wind mapping is a useful tool for offshore wind resource assessment because SAR data can provide observations of wind speed variation over coastal areas at a resolution relevant to the size of offshore wind farms (Beaucage et al. 2008; Hasager et al. 2005; Monaldo et al. 2014). The wind speed spatial pattern derived from SAR data was used to extrapolate in-situ measurements to create the Great Lake Wind Atlas (Doubrawa et al. 2015). While SAR data can provide good estimation of the annual mean wind speed, the limited sample number to date can introduce large uncertainty in estimating wind power density (Hasager et al. 2004; Hasager et al. 2011). Theoretical analyses show that, if the wind speed distribution is described using the Weibull distribution, about 70, 175 and 2000 samples are required to estimate the scale factor, the

shape factor and the power density with ±10% uncertainty at 95% confidence interval, respectively (Barthelmie and Pryor 2003; Pryor et al. 2004) assuming every scene is random in time and that wind speeds are accurately retrieved. The uncertainty in power density estimation can be reduced by adding climatological wind data from numeral models and scatterometers through the wind class method (Badger et al. 2010) and the strategic sampling approach (Beaucage et al. 2011). Note that SAR-based wind speed is at 10 m height; therefore, it needs to be extrapolated to the hub height for wind resource assessment. One approach to this employs the Monin-Obukhov length and the atmospheric boundary height from numerical models with a unified wind profile law (Badger et al. 2016; Badger et al. 2012).

In addition to wind resource assessment, the high resolution enables studies of mesoscale flow structures with SAR wind mapping. SAR data have been used to observe wake deficit of large offshore wind farms (Christiansen and Hasager 2005; Christiansen and Hasager 2006). The detected wake characteristics were consistent with in-situ observations and model predictions. Furthermore, it was found that wind speed deficit could extend to 5–20 km downstream of the wind farm depending on the atmospheric conditions and the number of wind turbines in operation. In addition to satellite-deployment, SAR has also been installed on aircraft and used to undertake measurements of flow variability in the coastal zone and whole wind-farm wakes downstream of the Horns Rev offshore wind farm (Hasager et al. 2013a).

5.2 Scatterometer

Scatterometers were developed to observe wind vectors over ocean surface using multiple antennas emitting and receiving microwave signals with different viewing angles relative to the wind direction. A detailed review of scatterometer applications can be found in (Liu 2002). Scatterometers have large swath widths; hence, they can provide two samples per day at one location. However, scatterometers have relatively low spatial resolution. For example, the SeaWinds scatterometer on NASA's QuickSCAT satellite, which has provided consistent and extensive wind data from 1999 to 2009 for global ocean wind research, has the swath of 1800 km and the spatial resolution of 25 km. Other scatterometers, such ASCAT and OSCAT, have the similar swath width and spatial resolution.

Wind speed and direction are estimated at 10 m height by fitting the observed NRCS to scatterometer specific GMFs and assuming neutral atmospheric conditions. Rain causes false high returns and introduce positive bias in wind speed because it changes sea surface and backscatters the radar microwave (Hilburn et al. 2006). Changes in sea surface temperature can cause variation in water viscosity and atmospheric stability and consequently cause uncertainty in wind retrieval. Ocean currents can also introduce errors in the retrieved wind speed (Dickinson et al. 2001). The error standard deviations of scatterometer-based wind speed and direction relative to buoy data and model simulations are about 1.5 m s^{-1} and 15°, respectively (Hasager et al. 2008; Wentz and Smith 1999; Winterfeldt et al. 2010). One of the most detailed evaluations of QuickSCAT measurements at three locations in the North Sea (conducted with sample sizes of several thousand individual measurements) found "mean biases (in situ minus satellite) are close to zero for wind speed and −2.7° for wind direction with a standard deviation of 1.2 m s^{-1} and 15° respectively" (Karagali et al. 2014).

Because of the coarse spatial resolution, scatterometer data are less suitable than SARs for wind farm sitting. NRCSs of pixels near the coast are affected by land surface and hence the derived winds speeds have large uncertainty and are insufficiently accurate for wind resource assessment (Furevik et al. 2011). However,

the fact that scatterometer-based wind data are frequent in time and available over the long term is valuable for offshore wind resource assessment. Studies have shown that wind data from scatterometers can provide extremely useful information about inter- and intra-annual variability of wind speed (see section 2) (Capps and Zender 2010; Furevik et al. 2011; Karagali et al. 2014; Karagali et al. 2013; Liu et al. 2008).

5.3 Best practice recommendations

Satellite remote sensing products have been used in a number of preliminary resource assessments but best practice recommendations for their use has yet to be codified in international standards. In terms of the community who use the satellite-based products for resource assessment the generally accepted trends and recommendations/best practice are:

- There is increased emphasis in terms of the state-of-the-art to integrate data from the different instrument suites into offshore wind resource estimates (Hasager et al. 2015).
- There is a high-degree of uncertainty in extrapolating from the measurement height for satellite products to the heights of relevance to the wind energy industry (Badger et al. 2016).
- SAR/scatterometer data can be used to develop initial wind resource maps and to characterize long-term variability in wind speeds, they should be used as guide to site an offshore meteorological mast or ground-based remote sensing instruments for detailed assessment (Hasager et al. 2008).

6 Summary and recommendations for future work

Offshore wind deployments have tremendous potential for expansion. For example, the European Wind Energy Association (EWEA) expects 150 GW of offshore wind capacity to be realized in 2030 (Wieczorek et al. 2013), and while the US market is more nascent there is a good resource (Schwartz et al. 2010), there are prospective developments in Massachusetts, Maryland, and Rhode Island waters and an ambitious goal 48 of 10 GW of installed offshore capacity by 2020 in the DoE 2020 plan (Archer et al. 2014). For large offshore wind farms large reductions in economic risk can be achieved by improvements in the accuracy of hub-height wind speed predictions. It has been reported that a decrease in the uncertainty in the sustained wind speed at hub-height of 0.1 ms^{-1} results in a saving worth about 10 million British pounds per year over the lifetime of the wind farm (Hasager et al. 2013b).

This report provides an overview of the variables required to fulfill power and load estimates for offshore wind farms and summarizes the types of measurement strategy that are currently available. While it is apparent that lidar-based technology is becoming the measurement technique of choice, other measurement strategies also have advantages. For example, making long-term measurements with vertical lidar is straight-forward in terms of data processing, and can measure above current wind turbine tip-heights, but its power requirement is much larger than that of a meteorological mast equipped with cup or sonic anemometers which could be operated to measure wind speeds accurately in the long-term. Similarly, although satellite-based remote sensing does not have the precision of mast-based anemometry or lidars, it does provide long-term assessment of wind speeds over very large areas than can be used to assess relative differences in time and space that would be prohibitively expensive ad logistically challenging using lidar or meteorological masts. Scanning lidar also has a role, particularly as it is starting to be used to quantify wind speeds over large areas – such as from the coast measuring offshore - but it is expensive and challenging in terms of data volume and processing. As also discussed herein, there is a continue need for development of best-practice guidelines for deployment and use of these new technologies within the wind energy industry.

There is a clear need for improved understanding of the marine boundary layer with a specific focus on the parameters describe above. Neutral stratification and a flat, smooth sea surface are routinely used as assumptions in offshore siting, but are not necessarily a conservative approach to resource estimation or to fatigue load calculations in offshore wind farms (Kalvig et al. 2014). Although there are purpose-built offshore support platforms (e.g. FINO (Muñoz-Esparza et al. 2012), and the proposed DoE facility at the Chesapeake Light Tower) and tall coastal masts (e.g. the National Test Station of Wind Turbines at Høvsøre, Denmark (Floors et al. 2013)), there is a clear need for additional structures in the offshore and coastal environment to allow measurements of wind profiles (through the hub-height and turbine rotor swept area) along with key observations of boundary layer height, and surface fluxes from in situ and ground-based remote sensing instruments. Critically such support structures must comply with current best practice in terms of instrumentation and minimization and careful characterization of flow distortion, and to have sufficient quantity and quality of power supply to enable deployment of a full suite of remote sensing instrumentation. Further, there is a need to transition from short-term field campaigns to making more representative (AKA long-term, multi-year continuous measurements) and for new methods to contextualize those measurements in the longer-term climate variability, and also to fully integrate measurements of the sea-surface (waves, ice etc, e.g. to better understand combine wind-wave loading

(Tarp-Johansen et al. 2006)). There is also a continuing need for measurements within operating offshore wind farms to better understand spatial variability of the flow and turbine-turbine interactions (Barthelmie and Pryor 2013) and array-array interactions (Hansen et al. 2015).

7 Bibliography

Afek, I., N. Sela, N. Narkiss, G. Shamai, and S. Tsadka, 2013: Wind measurement via direct detection lidar. *Proc. SPIE 8894, Lidar Technologies, Techniques, and Measurements for Atmospheric Remote Sensing IX, 889404,* doi:10.1117/1112.2031624.

Ahn, S., and J. A. Fessler, 2003: *Standard errors of mean, variance, and standard deviation estimators.* Technical Report, Communication and Signal Processing Lab, Department of EECS, University of Michigan.

Aitken, M. L., M. E. Rhodes, and J. K. Lundquist, 2012: Performance of a Wind-Profiling Lidar in the Region of Wind Turbine Rotor Disks. *J. Atmos. Oceanic Technol.*, **29,** 347-355.

Aitken, M. L., R. M. Banta, Y. L. Pichugina, and J. K. Lundquist, 2014: Quantifying Wind Turbine Wake Characteristics from Scanning Remote Sensor Data. *J. Atmos. Oceanic Technol.*, **31,** 765-787.

Archer, C. L., and Coauthors, 2014: Meteorology for coastal/offshore wind energy in the United States: Recommendations and research needs for the next 10 years. *Bulletin of the American Meteorological Society*, **95,** 515-519.

Aubinet, M., T. Vesala, and D. Papale, 2012: *Eddy covariance a practical guide to measurement and data analysis.* Springer, 450 pp.

Badger, M., J. Badger, M. Nielsen, C. B. Hasager, and A. Peña, 2010: Wind Class Sampling of Satellite SAR Imagery for Offshore Wind Resource Mapping. *Journal of Applied Meteorology and Climatology*, **49,** 2474-2491.

Badger, M., A. Peña, A. N. Hahmann, A. A. Mouche, and C. B. Hasager, 2016: Extrapolating satellite winds to turbine operating heights. *Journal of Applied Meteorology and Climatology*, **55,** 975-991.

Badger, M., and Coauthors, 2012: Bringing satellite winds to hub-height. *EWEA 2012-European Wind Energy Conference & Exhibition*, Copenhagen, Denmark.

Banakh, V., and I. Smalikho, 2013: *Coherent Doppler Wind Lidars in a Turbulent Atmosphere.* Artech House, 248 pp.

Banakh, V. A., I. N. Smalikho, F. Köpp, and C. Werner, 1999: Measurements of Turbulent Energy Dissipation Rate with a CW Doppler Lidar in the Atmospheric Boundary Layer. *J. Atmos. Oceanic Technol.*, **16,** 1044-1061.

Banta, R. M., Y. L. Pichugina, and W. A. Brewer, 2006: Turbulent velocity-variance profiles in the stable boundary layer generated by a nocturnal low-level jet. *J. Atmos. Sci.*, **63,** 2700-2719.

Banta, R. M., R. K. Newsom, J. K. Lundquist, Y. L. Pichugina, R. L. Coulter, and L. Mahrt, 2002: Nocturnal Low-Level Jet Characteristics Over Kansas During Cases-99. *Boundary-Layer Meteorology*, **105,** 221-252.

Barthelmie, R. J., and S. C. Pryor, 2003: Can satellite sampling of offshore wind speeds realistically represent wind speed distributions? *Journal of Applied Meteorology*, **42,** 83-94.

——, 2006: Challenges in Predicting Power Output from Offshore Wind Farms. *J. Energy Eng.*, **132,** 91-103.

Barthelmie, R. J., and L. E. Jensen, 2010: Evaluation of power losses due to wind turbine wakes at the Nysted offshore wind farm. *Wind Energy*, **13,** 573-586.

Barthelmie, R. J., and S. C. Pryor, 2013: Wake model evaluation using data from the Virtual Wakes Laboratory. *Applied Energy*, **104,** 834-844.

Barthelmie, R. J., A. M. Sempreviva, and S. C. Pryor, 2010: The influence of humidity fluxes on offshore wind speed profiles. *Annales Geophysicae*, **28,** 1043-1052.

Barthelmie, R. J., K. S. Hansen, and S. C. Pryor, 2013: Meteorological controls on wind turbine wakes. *Proceedings of the IEEE*, **101(4),** 1010-1019.

Barthelmie, R. J., M. S. Courtney, J. Højstrup, and S. E. Larsen, 1996: Meteorological aspects of offshore wind energy: Observations from the Vindeby wind farm. *Journal of Wind Engineering and Industrial Aerodynamics*, **62,** 191-211.

Barthelmie, R. J., B. Lange, A. M. S. Sempreviva, and O. Rathmann, 1999: Application of WAsP to offshore wind power prediction. *Proceedings of the 21st British Wind Energy Association Conference*, Cambridge, September 1999, Professional Engineering Publications, 301-310.

Barthelmie, R. J., J. Badger, S. C. Pryor, C. B. Hasager, M. B. Christiansen, and B. H. Jørgensen, 2007: Wind speed gradients in the coastal offshore environment: Issues pertaining to design and development of large offshore wind farms. *Wind Engineering*, **31,** 369-382.

Barthelmie, R. J., L. Folkerts, F. Ormel, P. Sanderhoff, P. Eecen, O. Stobbe, and N. M. Nielsen, 2003: Offshore wind turbine wakes measured by SODAR. *Journal of Atmospheric and Oceanic Technology*, **30,** 466-477.

Barthelmie, R. J., and Coauthors, 2006: Comparison of wake model simulations with offshore wind turbine wake profiles measured by sodar. *Journal of Atmospheric and Oceanic Technology*, **23(7),** 888-901.

Barthelmie, R. J., and Coauthors, 2005: Ten Years of Meteorological Measurements for Offshore Wind Farms. *Journal of Solar Energy Engineering*, **127,** 170-176.

Barthelmie, R. J., and Coauthors, 2014: 3D Wind and Turbulence Characteristics of the Atmospheric Boundary Layer. *Bulletin of the American Meteorological Society*, **95,** 743-756.

Beaucage, P., M. Bernier, G. Lafrance, and J. Choisnard, 2008: Regional Mapping of the Offshore Wind Resource: Towards a Significant Contribution From Space-Borne Synthetic Aperture Radars. *IEEE J. Sel. Top. Appl. Earth Observ. Remote Sens.*, **1,** 48-56.

Beaucage, P., G. Lafrance, J. Lafrance, J. Choisnard, and M. Bernier, 2011: Synthetic aperture radar satellite data for offshore wind assessment: A strategic sampling approach. *Journal of Wind Engineering and Industrial Aerodynamics*, **99,** 27-36.

Beljaars, A. C. M., 1987: The Influence of Sampling and Filtering on Measured Wind Gusts. *J. Atmos. Oceanic Technol.*, **4,** 613-626.

Berg, J., N. Vasiljevic, M. Kelly, G. Lea, and M. Courtney, 2015: Addressing Spatial Variability of Surface-Layer Wind with Long-Range WindScanners. *Journal of Atmospheric and Oceanic Technology*, **32,** 518-527.

Bingöl, F., J. Mann, and D. Foussekis, 2009: Conically scanning lidar error in complex terrain *Meteorologische Zeitschrift*, **18,** 189-195.

Boccippio, D. J., 1995: A Diagnostic Analysis of the VVP Single-Doppler Retrieval Technique. *J. Atmos. Oceanic Technol.*, **12,** 230-248.

Bousquet, O., and M. Chong, 1998: A Multiple-Doppler Synthesis and Continuity Adjustment Technique (MUSCAT) to Recover Wind Components from Doppler Radar Measurements. *J. Atmos. Oceanic Technol.*, **15,** 343-359.

Bradley, S., 2007: *Atmospheric acoustic remote sensing: principles and applications.* CRC Press, 296 pp.

Bradley, S., Y. Perrott, P. Behrens, and A. Oldroyd, 2012: Corrections for wind-speed errors from sodar and lidar in complex terrain. *Boundary-layer meteorology*, **143,** 37-48.

Branlard, E., and Coauthors, 2013: Retrieving wind statistics from average spectrum of continuous-wave lidar. *Atmos. Meas. Tech.*, **6,** 1673-1683.

Brock, F. V., and S. J. Richardson, 2001: *Meteorological measurement systems.* Oxford University Press, 304 pp.

Brower, M. C., 2012: *Wind Resource Assessment: A Practical Guide to Developing a Wind Project.* John Wiley & Sons, Inc., 280 pp.

Browning, K. A., and R. Wexler, 1968: The Determination of Kinematic Properties of a Wind Field Using Doppler Radar. *Journal of Applied Meteorology and Climatology*, **7,** 105-113.

Burton, T., D. Sharpe, N. Jenkins, and E. Bossanyi, 2011: *Wind energy handbook.* John Wiley & Sons, 780 pp.

Calhoun, R., R. Heap, M. Princevac, R. Newsom, H. Fernando, and D. Ligon, 2006: Virtual Towers Using Coherent Doppler Lidar during the Joint Urban 2003 Dispersion Experiment. *Journal of Applied Meteorology and Climatology*, **45,** 1116-1126.

Capps, S. B., and C. S. Zender, 2010: Estimated global ocean wind power potential from QuikSCAT observations, accounting for turbine characteristics and siting. *Journal of Geophysical Research: Atmospheres*, **115,** D09101.

Chai, T., C.-L. Lin, and R. K. Newsom, 2004: Retrieval of Microscale Flow Structures from High-Resolution Doppler Lidar Data Using an Adjoint Model. *J. Atmos. Sci.*, **61,** 1500-1520.

Charnock, H., 1955: Wind stress on a water surface. *Quarterly Journal of the Royal Meteorological Society*, **81,** 639.
Cherukuru, N. W., R. Calhoun, M. Lehner, S. W. Hoch, and C. D. Whiteman, 2015: Instrument configuration for dual-Doppler lidar coplanar scans: METCRAX II. *Journal of Applied Remote Sensing*, **9,** 096090-096090.
Cho, A., J. Kim, S. Lee, and C. Kee, 2011: Wind estimation and airspeed calibration using a UAV with a single-antenna GPS receiver and pitot tube. *IEEE transactions on aerospace and electronic systems*, **47,** 109-117.
Choukulkar, A., R. Calhoun, B. Billings, and J. Doyle, 2012: Investigation of a complex nocturnal flow in Owens valley, California using coherent Doppler lidar. *Boundary-layer meteorology*, **144,** 359-378.
Christiansen, M. B., and C. B. Hasager, 2005: Wake effects of large offshore wind farms identified from satellite SAR. *Remote Sensing of Environment*, **98,** 251-268.
Christiansen, M. B., and C. B. Hasager, 2006: Using airborne and satellite SAR for wake mapping offshore. *Wind Energy*, **9,** 437-455.
Christiansen, M. B., W. Koch, J. Horstmann, C. B. Hasager, and M. Nielsen, 2006: Wind resource assessment from C-band SAR. *Remote Sensing of Environment*, **105,** 68-81.
Clifton, A., 2015: *Remote Sensing of Complex Flows by Doppler Wind Lidar: Issues and Preliminary Recommendations.* National Renewable Energy Laboratory, NREL/TP-5000-64634.
Clifton, A., D. Elliott, and M. S. Courtney, 2013: Ground-Based Vertically Profiling Remote Sensing For Wind Resource Assessment.
Clive, P., 2011a: Remote sensing best practice. *EWEA Offshore*, PO.0322.
——, 2011b: Remote sensing standards: their current standards and significance for offshore projects. *EWEA Offshore*, PO.009.
Coles, S., J. Bawa, L. Trenner, and P. Dorazio, 2001: *An introduction to statistical modeling of extreme values.* Vol. 208, Springer, 219 pp.
Collier, C. G., and Coauthors, 2005: Dual-Doppler Lidar Measurements for Improving Dispersion Models. *Bulletin of the American Meteorological Society*, **86,** 825-838.
Cooperman, A., and M. Martinez, 2015: Load monitoring for active control of wind turbines. *Renewable and Sustainable Energy Reviews*, **41,** 189-201.
Coquilla, R. V., A. Havner, J. Obermeier, and M. Sturgeon, 2010: Verification testing of Sonic anemometer wind speed measurements for wind energy applications. *Proceedings of the 2010 American Wind Energy Association Annual Conference (AWEA WINDPOWER'10)*, 1-14.
Courtney, M. S., and C. B. Hasager, 2016: 4 - Remote sensing technologies for measuring offshore wind. *Offshore Wind Farms*, Woodhead Publishing, 59-82.
Dagestad, K.-F., and Coauthors, 2013: Wind retrieval from synthetic aperture radar-an overview. *Proceedings of SEASAR 2012, 4th SAR Oceanography Workshop (SEASAR 2012)*, Tromsø, Norway, 22.
Dickinson, S., K. A. Kelly, M. J. Caruso, and M. J. McPhaden, 2001: Comparisons between the TAO Buoy and NASA Scatterometer Wind Vectors. *J. Atmos. Oceanic Technol.*, **18,** 799-806.
Dimitrov, N., A. Natarajan, and M. Kelly, 2015: Model of wind shear conditional on turbulence and its impact on wind turbine loads. *Wind Energy*, **18,** 1917-1931.
DNV, 2011: Use of remote sensing for wind energy assessments.
Doubrawa, P., R. J. Barthelmie, S. C. Pryor, C. B. Hasager, M. Badger, and I. Karagali, 2015: Satellite winds as a tool for offshore wind resource assessment: The Great Lakes Wind Atlas. *Remote Sensing of Environment*, **168,** 349-359.
Doviak, R. J., and D. S. Zrnić, 1993: *Doppler Radar and Weather Observations (Second Edition).* Academic Press, 562 pp.
Drechsel, S., G. J. Mayr, M. Chong, M. Weissmann, A. Dörnbrack, and R. Calhoun, 2009: Three-Dimensional Wind Retrieval: Application of MUSCAT to Dual-Doppler Lidar. *J. Atmos. Oceanic Technol.*, **26,** 635-646.
Ecofys, 2013: Improved Bankability. The Ecofys position on LiDAR use. http://www.ecofys.com/files/files/ecofys-2013-position-paper-on-lidar-use_02.pdf Accessed 8 July 2016.

Eecen, P., and M. d. Noord, 2005: *Uncertainties in Cup Anemometer Calibrations: Type A and Type B uncertainties. ECN: Wind Energy, ECN-C--05-066.* Vol. 2012, 62 pp pp.
Emeis, S., 2010: *Measurement Methods in Atmospheric Sciences.* Schweizerbart Science Publishers, 275 pp.
Emeis, S., 2011: *Surface-Based Remote Sensing of the Atmospheric Boundary Layer.* Springer, 174 pp.
Emeis, S., 2012: *Wind energy meteorology atmospheric physics for wind power generation.* Springer, 196 pp.
Emeis, S., 2014: Current issues in wind energy meteorology. *Meteorological Applications*, **21,** 803-819.
Emeis, S., M. Harris, and R. M. Banta, 2007: Boundary-layer anemometry by optical remote sensing for wind energy applications. *Meteorologische Zeitschrift*, **16,** 337-347.
Emeis, S., K. Schäfer, and C. Münkel, 2008: Surface-based remote sensing of the mixing-layer height – a review. *Meteorologische Zeitschrift*, **17,** 621-630.
Enloe, J., J. J. O'Brien, and S. R. Smith, 2004: ENSO Impacts on Peak Wind Gusts in the United States. *Journal of Climate*, **17,** 1728-1737.
Ernst, B., and J. R. Seume, 2012: Investigation of Site-Specific Wind Field Parameters and Their Effect on Loads of Offshore Wind Turbines. *Energies*, **5,** 3835-3855.
Fabre, S., M. Stickland, T. Scanlon, A. Oldroyd, D. Kindler, and F. Quail, 2014: Measurement and simulation of the flow field around the FINO 3 triangular lattice meteorological mast. *Journal of Wind Engineering and Industrial Aerodynamics*, **130,** 99-107.
Farrugia, R. N., and T. Sant, 2013: Modelling wind speeds for cup anemometers mounted on opposite sides of a lattice tower: A case study. *Journal of Wind Engineering and Industrial Aerodynamics*, **115,** 173-183.
Fichaux, N., and T. Ranchin, 2002: Combined extraction of high spatial resolution wind speed and wind direction from SAR images: A new approach using wavelet transform. *Canadian Journal of Remote Sensing*, **28,** 510-516.
Filippelli, M., J. Bouget, M. Brower, and D. Bernadett, 2008: Adjustment of Anemometer Readings for Energy Production Estimates. AWS Truewind. *AWEA WINDPOWER*, Houston, TX.
Floors, R., C. L. Vincent, S.-E. Gryning, A. Peña, and E. Batchvarova, 2013: The wind profile in the coastal boundary layer: wind lidar measurements and numerical modelling. *Boundary-layer meteorology*, **147,** 469-491.
Frehlich, R., and M. Yadlowsky, 1994: Performance of mean-frequency estimators for Doppler radar and lidar. *J. Atmos. Oceanic Technol.*, **11,** 1217-1230.
Frehlich, R., and L. Cornman, 2002: Estimating Spatial Velocity Statistics with Coherent Doppler Lidar. *J. Atmos. Oceanic Technol.*, **19,** 355-366.
Friis Pedersen, T., J.-Å. Dahlberg, and P. Busche, 2006: ACCUWIND - Classification of five cup anemometers according to IEC 61400-12-1. (Denmark. Forskningscenter Risoe. Risoe-R; No. 1556(EN)). 72 pp pp.
Furevik, B. R., O. M. Johannessen, and A. D. Sandvik, 2002: SAR-retrieved wind in polar regions-comparison with in situ data and atmospheric model output. *IEEE Transactions on Geoscience and Remote Sensing*, **40,** 1720-1732.
Furevik, B. R., A. M. Sempreviva, L. Cavaleri, J.-M. Lefèvre, and C. Transerici, 2011: Eight years of wind measurements from scatterometer for wind resource mapping in the Mediterranean Sea. *Wind Energy*, **14,** 355-372.
Gal-Chen, T., M. Xu, and W. L. Eberhard, 1992: Estimations of atmospheric boundary layer fluxes and other turbulence parameters from Doppler lidar data. *Journal of Geophysical Research: Atmospheres*, **97,** 18409-18423.
Garratt, J. R., 1990: The internal boundary layer - a review. *Boundary-Layer Meteorology*, **50,** 171-203.
GLGH, 2012: GL GH position statement on WINDCUBE remote sesnsing device, 11 pp.
González, J. S., M. B. Payán, J. M. R. Santos, and F. González-Longatt, 2014: A review and recent developments in the optimal wind-turbine micro-siting problem. *Renewable and Sustainable Energy Reviews*, **30,** 133-144.

Goodberlet, M., C. Swift, and J. Wilkerson, 1989: Remote sensing of ocean surface winds with the Special Sensor Microwave/Imager. *Journal of Geophysical Research: Oceans*, **94,** 14547-14555.
Gottschall, J., M. S. Courtney, R. Wagner, H. E. Jørgensen, and I. Antoniou, 2012: Lidar profilers in the context of wind energy–a verification procedure for traceable measurements. *Wind Energy*, **15,** 147-159.
Grelle, A., and A. Lindroth, 1994: Flow Distortion by a Solent Sonic Anemometer: Wind Tunnel Calibration and Its Assessment for Flux Measurements over Forest and Field. *J. Atmos. Oceanic Technol.*, **11,** 1529-1542.
Grilli, A. R., and M. L. Spaulding, 2013: Offshore Wind Resource Assessment in Rhode Island Waters. *Wind Engineering*, **37,** 579-594.
Gryning, S.-E., E. Batchvarova, B. Brümmer, H. Jørgensen, and S. Larsen, 2007: On the extension of the wind profile over homogeneous terrain beyond the surface boundary layer. *Boundary-Layer Meteorology*, **124,** 251-268.
Hahmann, A. N., C. L. Vincent, A. Peña, J. Lange, and C. B. Hasager, 2015: Wind climate estimation using WRF model output: method and model sensitivities over the sea. *International Journal of Climatology*, **35,** 3422-3439.
Hansen, K. S., and Coauthors, 2015: Simulation of wake effects between two wind farms. *Journal of Physics: Conference Series*, **625,** 012008.
Hansen, M. O., and B. Pedersen, 1999: Influence of the meteorology mast on a cup anemometer. *Journal of solar energy engineering*, **121,** 128-131.
Hasager, C. B., E. Dellwik, M. Nielsen, and B. R. Furevik, 2004: Validation of ERS-2 SAR offshore wind-speed maps in the North Sea. *International Journal of Remote Sensing*, **25,** 3817-3841.
Hasager, C. B., M. Badger, P. Astrup, and I. Karagali, 2013a: Satellite Remote Sensing in Offshore Wind Energy. *Handbook of Wind Power Systems*, M. P. Pardalos, S. Rebennack, F. M. V. Pereira, A. N. Iliadis, and V. Pappu, Eds., Springer Berlin Heidelberg, 711-745.
Hasager, C. B., M. Badger, A. Peña, X. G. Larsén, and F. Bingöl, 2011: SAR-based wind resource statistics in the Baltic Sea. *Remote Sensing*, **3,** 117-144.
Hasager, C. B., D. Stein, M. Courtney, A. Peña, T. Mikkelsen, M. Stickland, and A. Oldroyd, 2013b: Hub height ocean winds over the North Sea observed by the NORSEWInD lidar array: measuring techniques, quality control and data management. *Remote Sensing*, **5,** 4280-4303.
Hasager, C. B., and Coauthors, 2008: Remote Sensing Observation Used in Offshore Wind Energy. *IEEE Journal of Selected Topics in Applied Earth Observations and Remote Sensing*, **1,** 67-79.
Hasager, C. B., and Coauthors, 2015: Offshore wind climatology based on synergetic use of Envisat ASAR, ASCAT and QuikSCAT. *Remote Sensing of Environment*, **156,** 247-263.
Hasager, C. B., and Coauthors, 2005: Offshore wind resource estimation from satellite SAR wind field maps. *Wind Energy*, **8,** 403-419.
He, Y., W. Perrie, Q. Zou, and P. W. Vachon, 2005: A new wind vector algorithm for C-band SAR. *IEEE Transactions on Geoscience and Remote Sensing*, **43,** 1453-1458.
Hersbach, H., A. Stoffelen, and S. de Haan, 2007: An improved C-band scatterometer ocean geophysical model function: CMOD5. *Journal of Geophysical Research: Oceans*, **112,** C03006.
Hilburn, K. A., F. J. Wentz, D. K. Smith, and P. D. Ashcroft, 2006: Correcting Active Scatterometer Data for the Effects of Rain Using Passive Radiometer Data. *Journal of Applied Meteorology and Climatology*, **45,** 382-398.
Hill, M., and Coauthors, 2010: Coplanar Doppler Lidar Retrieval of Rotors from T-REX. *J. Atmos. Sci.*, **67,** 713-729.
Hirth, B. D., J. L. Schroeder, W. S. Gunter, and J. G. Guynes, 2015: Coupling Doppler radar‐derived wind maps with operational turbine data to document wind farm complex flows. *Wind Energy*, **18,** 529-540.
Högström, U., and A.-S. Smedman, 2004: Accuracy of Sonic Anemometers: Laminar Wind-Tunnel Calibrations Compared to Atmospheric In Situ Calibrations Against a Reference Instrument. *Boundary-Layer Meteorology*, **111,** 33-54.
Holmes, J. D., 2001: *Wind loading of structures.* CRC Press.

Holtslag, M. C., W. A. A. M. Bierbooms, and G. J. W. van Bussel, 2015: Validation of surface layer similarity theory to describe far offshore marine conditions in the Dutch North Sea in scope of wind energy research. *Journal of Wind Engineering and Industrial Aerodynamics*, **136,** 180-191.

Huffaker, R. M., and R. M. Hardesty, 1996: Remote sensing of atmospheric wind velocities using solid-state and CO2 coherent laser systems. *Proceedings of the IEEE*, **84,** 181-204.

IEC, 2005a: IEC 61400-1: Wind turbines part 1: Design requirements. *International Electrotechnical Commission*, 177.

——, 2005b: IEC 61400-12-1: 2005 Wind turbines - Part 12-1: Power performance measurements of electricity producing wind turbines. 90.

——, 2009: IEC 61400-3. *Wind turbines Part 3: Design requirements for offshore wind turbines*, 263.

Islam, M., S. Mekhilef, and R. Saidur, 2013: Progress and recent trends of wind energy technology. *Renewable and Sustainable Energy Reviews*, **21,** 456-468.

Kaldellis, J., and M. Kapsali, 2013: Shifting towards offshore wind energy—Recent activity and future development. *Energy Policy*, **53,** 136-148.

Kalvig, S., O. T. Gudmestad, and N. Winther, 2014: Exploring the gap between 'best knowledge'and 'best practice'in boundary layer meteorology for offshore wind energy. *Wind Energy*, **17,** 161-171.

Karagali, I., A. Peña, M. Badger, and C. B. Hasager, 2014: Wind characteristics in the North and Baltic Seas from the QuikSCAT satellite. *Wind Energy*, **17,** 123-140.

Karagali, I., M. Badger, A. N. Hahmann, A. Peña, C. B. Hasager, and A. M. Sempreviva, 2013: Spatial and temporal variability of winds in the Northern European Seas. *Renewable energy*, **57,** 200-210.

Kim, M. G., and P. H. Dalhoff, 2014: Yaw Systems for wind turbines – Overview of concepts, current challenges and design methods. *J. Phys.: Conf. Ser.*, **524,** 012086.

Koch, G. J., and Coauthors, 2012: Side-scan Doppler lidar for offshore wind energy applications. *Journal of Applied Remote Sensing*, **6,** 063562.

Koch, W., 2004: Directional analysis of SAR images aiming at wind direction. *IEEE Transactions on Geoscience and Remote Sensing*, **42,** 702-710.

Kochendorfer, J., T. P. Meyers, J. Frank, W. J. Massman, and M. W. Heuer, 2012: How Well Can We Measure the Vertical Wind Speed? Implications for Fluxes of Energy and Mass. *Boundary-Layer Meteorology*, **145,** 383-398.

Köpp, F., S. Rahm, and I. Smalikho, 2004: Characterization of Aircraft Wake Vortices by 2-µm Pulsed Doppler Lidar. *J. Atmos. Oceanic Technol.*, **21,** 194-206.

Krishnamurthy, R., A. Choukulkar, R. Calhoun, J. Fine, A. Oliver, and K. S. Barr, 2013: Coherent Doppler lidar for wind farm characterization. *Wind Energy*, **16,** 189-206.

Kristensen, L., 1993: *The cup anemometer and other exciting instruments.* . Risoe National Laboratory. Riso-R-615(EN), 82 pp.

Kuhn, M., D. Trabucchi, and A. Clifton, 2015: IEA Task 32: Wind Lidar Systems for Wind Energy Deployment (LIDAR), 27 pp.

Kyaw Tha Paw, U., D. D. Baldocchi, T. P. Meyers, and K. B. Wilson, 2000: Correction Of Eddy-Covariance Measurements Incorporating Both Advective Effects And Density Fluxes. *Boundary-Layer Meteorology*, **97,** 487-511.

Lang, S., and E. McKeogh, 2011: LIDAR and SODAR measurements of wind speed and direction in upland terrain for wind energy purposes. *Remote Sensing*, **3,** 1871-1901.

Lange, B., S. Larsen, J. Højstrup, and R. Barthelmie, 2004: Importance of thermal effects and sea surface roughness for offshore wind resource assessment. *Journal of Wind Engineering and Industrial Aerodynamics*, **92,** 959-988.

Lantz, E., R. Wiser, and M. Hand, 2012: The past and future cost of wind energy. *National Renewable Energy Laboratory, Golden, CO, Report No. NREL/TP-6A20-53510*.

Larsen, G. C., and K. S. Hansen, 2008: Rational calibration of four IEC 61400-1 extreme external conditions. *Wind Energy*, **11,** 685-702.

Larsén, X. G., J. Badger, A. N. Hahmann, and N. G. Mortensen, 2013: The selective dynamical downscaling method for extreme‐wind atlases. *Wind Energy*, **16,** 1167-1182.
Larsén, X. G., C. Kalogeri, G. Galanis, and G. Kallos, 2015: A statistical methodology for the estimation of extreme wave conditions for offshore renewable applications. *Renewable Energy*, **80,** 205-218.
Lenschow, D. H., J. Mann, and L. Kristensen, 1994: How Long Is Long Enough When Measuring Fluxes and Other Turbulence Statistics? *J. Atmos. Oceanic Technol.*, **11,** 661-673.
Lindelöw, P., M. Courtney, R. Parmentier, and J. Cariou, 2008: Wind shear proportional errors in the horizontal wind speed sensed by focused, range gated lidars. *IOP Conference Series: Earth and Environmental Science*, IOP Publishing, 012023.
Liu, W. T., 2002: Progress in Scatterometer Application. *Journal of Oceanography*, **58,** 121-136.
Liu, W. T., W. Tang, and X. Xie, 2008: Wind power distribution over the ocean. *Geophys. Res. Lett.*, **35,** L13808.
Mahrt, L., D. Vickers, and E. Moore, 2004: Flow adjustments across sea-surface temperature changes. *Boundary-layer meteorology*, **111,** 553-564.
Mahrt, L., D. Vickers, and E. L. Andreas, 2013: Low-Level Wind Maxima and Structure of the Stably Stratified Boundary Layer in the Coastal Zone, . *Journal of Applied Meteorology and Climatology*, **53,** 363-376. doi: 310.1175/JAMC-D-1113-0170.1171.
Mann, J., 1994: The spatial structure of neutral atmospheric surface-layer turbulence. *Journal of Fluid Mechanics*, **273,** 141-168.
Mann, J., A. Peña, F. Bingöl, R. Wagner, and M. S. Courtney, 2010: Lidar Scanning of Momentum Flux in and above the Atmospheric Surface Layer. *J. Atmos. Oceanic Technol.*, **27,** 959-976.
Marshall, J., and Coauthors, 2001: North Atlantic climate variability: phenomena, impacts and mechanisms. *International Journal of Climatology*, **21,** 1863-1898.
Mathisen, J.-P., 2013: Measurement of wind profile with a buoy mounted lidar. *Energy Procedia/Proceedings of DeepWind Conference*.
Mears, C., D. K. Smith, and F. J. Wentz, 2001: Comparison of Special Sensor Microwave Imager and buoy-measured wind speeds from 1987 to 1997. *Journal of Geophysical Research*, **106,** 11719-11729.
MEASNET, 2009: Evaluation of site specific wind conditions, 53 pp.
Mikkelsen, T., 2014: Lidar-based research and innovation at DTU wind energy–a review. *J. Phys.: Conf. Ser.*, IOP Publishing, 012007.
Monahan, A. H., 2011: Can We See the Wind? Statistical Downscaling of Historical Sea Surface Winds in the Subarctic Northeast Pacific. *Journal of Climate*, **25,** 1511-1528.
Monaldo, F. M., X. Li, W. G. Pichel, and C. R. Jackson, 2014: Ocean Wind Speed Climatology from Spaceborne SAR Imagery. *Bulletin of the American Meteorological Society*, **95,** 565-569.
Muñoz-Esparza, D., B. Cañadillas, T. Neumann, and J. van Beeck, 2012: Turbulent fluxes, stability and shear in the offshore environment: Mesoscale modelling and field observations at FINO1. *Journal of Renewable and Sustainable Energy*, **4,** 063136.
Nakai, T., and K. Shimoyama, 2012: Ultrasonic anemometer angle of attack errors under turbulent conditions. *Agricultural and Forest Meteorology*, **162–163,** 14-26.
Newman, J. F., P. M. Klein, S. Wharton, A. Sathe, T. A. Bonin, P. B. Chilson, and A. Muschinski, 2016: Evaluation of three lidar scanning strategies for turbulence measurements. *Atmos. Meas. Tech.*, **9,** 1993-2013.
Newsom, R. K., L. K. Berg, W. J. Shaw, and M. L. Fischer, 2015: Turbine-scale wind field measurements using dual-Doppler lidar. *Wind Energy*, **18,** 219-235.
Nunalee, C. G., and S. Basu, 2014: Mesoscale modeling of coastal low-level jets: implications for offshore wind resource estimation. *Wind Energy*, **17,** 1199-1216.
Palutikof, J. P., B. B. Brabson, D. H. Lister, and S. T. Adcock, 1999: A review of methods to calculate extreme wind speeds. *Meteorological Applications*, **6,** 119-132.

Papadopoulos, K. H., N. C. Stefantos, U. S. Paulsen, and E. Morfiadakis, 2001: Effects of Turbulence and Flow Inclination on the Performance of Cup Anemometers in the Field. *Boundary-Layer Meteorology*, **101,** 77-107.

Paulsen, U. S., N. G. Mortensen, J. C. Hansen, U. S. Said, and A. Moussa, 2007: Field calibration of cup anemometers. *Conference proceedings (online) 2007 European Wind Energy Conference and Exhibition, Milan (IT)*, 7-10.

Pearson, G. N., and C. G. Collier, 1999: A pulsed coherent CO2 lidar for boundary-layer meteorology. *Quarterly Journal of the Royal Meteorological Society*, **125,** 2703-2721.

Pedersen, F. T., J. Å. Dahlberg, and P. Busche, 2006: ACCUWIND-Classification of five cup anemometers according to IEC 61400-12-1Risoe 1556(EN), 2006.

Peña, A., S.-E. Gryning, and R. R. Floors, 2015a: Lidar observations of marine boundary-layer winds and heights: a preliminary study. *Meteorologische Zeitschrift*, **24,** 581-589.

Peña, A., C. B. Hasager, S. E. Gryning, M. Courtney, I. Antoniou, and T. Mikkelsen, 2009: Offshore wind profiling using light detection and ranging measurements. *Wind Energy*, **12,** 105-124.

Peña, A., and Coauthors, 2015b: Ten Years of Boundary-Layer and Wind-Power Meteorology at Høvsøre, Denmark. *Boundary-Layer Meteorology*, **158,** 1-26.

Pichugina, Y. L., R. M. Banta, W. A. Brewer, S. P. Sandberg, and R. M. Hardesty, 2012: Doppler Lidar-Based Wind-Profile Measurement System for Offshore Wind-Energy and Other Marine Boundary Layer Applications. *Journal of Applied Meteorology and Climatology*, **51,** 327-349.

Pindado, S., A. Barrero-Gil, and A. Sanz, 2012: Cup Anemometers' Loss of Performance Due to Ageing Processes, and Its Effect on Annual Energy Production (AEP) Estimates. *Energies*, **5,** 1664-1685.

Poulsen, T., and C. B. Hasager, 2016: How Expensive Is Expensive Enough? Opportunities for Cost Reductions in Offshore Wind Energy Logistics. *Energies*, **9,** 437.

Pryor, S. C., and R. J. Barthelmie, 2001: Comparison of potential power production at on- and off-shore sites. *Wind Energy*, **4,** 173-181.

——, 2002: Statistical analysis of flow characteristics in the coastal zone. *Journal of Wind Engineering and Industrial Aerodynamics*, **90,** 201-221.

——, 2003: Long‐term trends in near‐surface flow over the Baltic. *International Journal of Climatology*, **23,** 271-289.

Pryor, S. C., R. J. Barthelmie, and J. T. Schoof, 2006: Inter-annual variability of wind indices across Europe. *Wind Energy*, **9,** 27-38.

Pryor, S. C., M. Nielsen, R. J. Barthelmie, and J. Mann, 2004: Can satellite sampling of offshore wind speeds realistically represent wind speed distributions? Part II: Quantifying uncertainties associated with sampling strategy and distribution fitting methods. *Journal of Applied Meteorology*, **43,** 739-750.

Pryor, S. C., R. J. Barthelmie, N. E. Clausen, M. Drews, N. MacKellar, and E. Kjellstrom, 2012: Analyses of possible changes in intense and extreme wind speeds over northern Europe under climate change scenarios. *Climate Dynamics*, **38,** 189-208, doi: 110.1007/s00382-00010-00955-00383.

Ranjha, R., G. Svensson, M. Tjernström, and A. Semedo, 2013: Global distribution and seasonal variability of coastal low-level jets derived from ERA-Interim reanalysis. *2013*, **65,** doi: 10.3402/tellusa.v3465i3400.20412.

Rodrigo, J. S., F. B. Guillén, P. G. Arranz, M. Courtney, R. Wagner, and E. Dupont, 2013: Multi-site testing and evaluation of remote sensing instruments for wind energy applications. *Renewable Energy*, **53,** 200-210.

Rodrigues, S., C. Restrepo, E. Kontos, R. T. Pinto, and P. Bauer, 2015: Trends of offshore wind projects. *Renewable and Sustainable Energy Reviews*, **49,** 1114-1135.

RSI, 1995: *RADARSAT illuminated : your guide to products and services*. RADARSAT International British Columbia, Canada.

Sathe, A., and J. Mann, 2013: A review of turbulence measurements using ground-based wind lidars. *Atmos. Meas. Tech.*, **6,** 3147-3167.

Sathe, A., J. Mann, J. Gottschall, and M. S. Courtney, 2011: Can Wind Lidars Measure Turbulence? *Journal of Atmospheric and Oceanic Technology*, **28,** 853-868.
Sathe, A., J. Mann, N. Vasiljevic, and G. Lea, 2015: A six-beam method to measure turbulence statistics using ground-based wind lidars. *Atmos. Meas. Tech.*, **8,** 729-740.
Sathe, A., J. Mann, T. Barlas, W. Bierbooms, and G. Bussel, 2013: Influence of atmospheric stability on wind turbine loads. *Wind Energy*, **16,** 1013-1032.
Schoof, J. T., and S. C. Pryor, 2014: Assessing the fidelity of AOGCM‐simulated relationships between large‐scale modes of climate variability and wind speeds. *Journal of Geophysical Research: Atmospheres*, **119,** 9719-9734.
Schwartz, M., D. Heimiller, S. Haymes, and W. Musial, 2010: Assessment of offshore wind energy resources for the United States. *National Renewable Energy Lab. Golden, CO, Technical Report No. NREL/TP-500-45889*.
Sempreviva, A. M., R. J. Barthelmie, and S. C. Pryor, 2009: Review of methodologies for offshore wind resource assessment in European Seas. *Surveys in Geophysics*, **DOI 10.1007/s 10712-008-9050-2,** 27.
Shaw, W., 2012: Offshore Resource Assessment and Design Conditions: A Data Requirements and Gaps Analysis for Offshore Renewable Energy Systems.
Simley, E., L. Y. Pao, R. Frehlich, B. Jonkman, and N. Kelley, 2014: Analysis of light detection and ranging wind speed measurements for wind turbine control. *Wind Energy*, **17,** 413-433.
Smedman, A. S., U. Hogstrom, and H. Bergstrom, 1996: Low level jets - a decisive factor for off-shore wind energy siting in the Baltic Sea. *Wind Engineering*, **20,** 137-147.
Sonnensc, C. M., and F. A. Horrigan, 1971: Signal-to-noise relationships for coaxial systems that heterodyne backscatter from atmosphere. *Applied Optics*, **10,** 1600-&.
Stawiarski, C., K. Träumner, C. Knigge, and R. Calhoun, 2013: Scopes and Challenges of Dual-Doppler Lidar Wind Measurements—An Error Analysis. *J. Atmos. Oceanic Technol.*, **30,** 2044-2062.
Stawiarski, C., K. Träumner, C. Kottmeier, C. Knigge, and S. Raasch, 2015: Assessment of Surface-Layer Coherent Structure Detection in Dual-Doppler Lidar Data Based on Virtual Measurements. *Boundary-Layer Meteorology*, **156,** 371-393.
Stoffelen, A., and D. Anderson, 1997: Scatterometer data interpretation: Estimation and validation of the transfer function CMOD4. *Journal of Geophysical Research: Oceans*, **102,** 5767-5780.
Storey, R., S. Norris, and J. Cater, 2014: Modelling turbine loads during an extreme coherent gust using large eddy simulation. *J. Phys.: Conf. Ser.*, IOP Publishing, 012177.
Stull, R. B., 1988: *An introduction to boundary layer meteorology*. Vol. 13, Springer Science & Business Media, 670 pp.
Sun, X. J., D. G. Huang, and G. Q. Wu, 2012: The current state of offshore wind energy technology development. *Energy*, **41,** 298-312.
Tarp-Johansen, N., J. Manwell, and J. McGowan, 2006: Application of design standards to the design of offshore wind turbines in the US. *Offshore Technology Conference*.
Thomsen, K., 2014: *Offshore Wind, Second Edition: A Comprehensive Guide to Successful Offshore Wind Farm Installation* Academic Press.
Trager, E. C., 2014: Case Studies From Implementation of the First Commercial Leasing Processes for Areas of the Outer Continental Shelf (OCS) Under the US Renewable Energy Regulations, 30 CFR 585. *ASME 2014 33rd International Conference on Ocean, Offshore and Arctic Engineering*, American Society of Mechanical Engineers, V09AT09A031-V009AT009A031.
Trombe, P.-J., and Coauthors, 2014: Weather radars – the new eyes for offshore wind farms? *Wind Energy*, **17,** 1767-1787.
Türk, M., and S. Emeis, 2010: The dependence of offshore turbulence intensity on wind speed. *Journal of Wind Engineering and Industrial Aerodynamics*, **98,** 466-471.
van Hulle, F., N. Fichaux, A. Sinner, F. E. Morthorst, and J. Munksgaard, 2010: *Powering Europe: wind energy and the electricity grid.* European Wind Energy Association, 179 pp.

Vasiljevic, N., 2014: A time-space synchronization of coherent Doppler scanning lidars for 3D measurements of wind fields, Department of Wind Energy, Technical University of Denmark.
Vickers, D., and L. Mahrt, 2006: Contrasting mean vertical motion from tilt correction methods and mass continuity. *Agricultural and Forest Meteorology*, **138,** 93-103.
Wagner, R., I. Antoniou, S. M. Pedersen, M. S. Courtney, and H. E. Jørgensen, 2009: The influence of the wind speed profile on wind turbine performance measurements. *Wind Energy*, **12,** 348-362.
Wagner, R., T. F. Pedersen, M. Courtney, I. Antoniou, S. Davoust, and R. L. Rivera, 2014: Power curve measurement with a nacelle mounted lidar. *Wind Energy*, **17,** 1441-1453.
Wang, H., and R. J. Barthelmie, 2015: Wind turbine wake detection with a single Doppler wind lidar. *J. Phys.: Conf. Ser.*, **625,** 012017.
Wang, H., R. J. Barthelmie, S. C. Pryor, and H. G. Kim, 2014: A new turbulence model for offshore wind turbine standards. *Wind Energy*, **17,** 1587-1604.
Wang, H., R. J. Barthelmie, A. Clifton, and S. C. Pryor, 2015: Wind Measurements from Arc Scans with Doppler Wind Lidar. *J. Atmos. Oceanic Technol.*, **32,** 2024-2040.
Wang, H., R. J. Barthelmie, S. C. Pryor, and Brown, 2016a: Lidar arc scan uncertainty reduction through scanning geometry optimization. *Atmos. Meas. Tech.*, **9,** 1653-1669.
Wang, H., R. J. Barthelmie, P. Doubrawa, and S. C. Pryor, 2016b: Errors in radial velocity variance from Doppler wind lidar. *Atmospheric Measurement Techniques Discussions*, **In review doi:10.5194/amt-2016-83**.
Wang, Y., and Coauthors, 2016c: Triple Doppler wind lidar observations during the mountain terrain atmospheric modeling and observations field campaign. *Journal of Applied Remote Sensing*, **10,** 026015-026015.
Weissmann, M., A. Dörnbrack, and J. D. Doyle, 2009: Vorticity from Line-of-Sight Lidar Velocity Scans. *J. Atmos. Oceanic Technol.*, **26,** 2683-2690.
Wentz, F. J., and D. K. Smith, 1999: A model function for the ocean-normalized radar cross section at 14 GHz derived from NSCAT observations. *Journal of Geophysical Research: Oceans*, **104,** 11499-11514.
Westerhellweg, A., T. Neumann, and V. Riedel, 2012: Fino1 mast correction. *Dewi magazin*, 3.
Wieczorek, A. J., S. O. Negro, R. Harmsen, G. J. Heimeriks, L. Luo, and M. P. Hekkert, 2013: A review of the European offshore wind innovation system. *Renewable and Sustainable Energy Reviews*, **26,** 294-306.
Wilczak, J. M., S. P. Oncley, and S. A. Stage, 2001: Sonic Anemometer Tilt Correction Algorithms. *Boundary-Layer Meteorology*, **99,** 127-150.
Winterfeldt, J., A. Andersson, C. Klepp, S. Bakan, and R. Weisse, 2010: Comparison of HOAPS, QuikSCAT, and Buoy Wind Speed in the Eastern North Atlantic and the North Sea. *IEEE Transactions on Geoscience and Remote Sensing*, **48,** 338-348.
Wyngaard, J. C., 1981: Cup, Propeller, Vane, and Sonic Anemometers in Turbulence Research. *Annual Review of Fluid Mechanics*, **13,** 399-423.
Xia, Q., C.-L. Lin, R. Calhoun, and R. K. Newsom, 2008: Retrieval of Urban Boundary Layer Structures from Doppler Lidar Data. Part I: Accuracy Assessment. *J. Atmos. Sci.*, **65,** 3-20.

